JGR Space Physics

RESEARCH ARTICLE
10.1029/2025JA033942

Parametric Regimes of Thin Current Sheets in Planetary Magnetospheres and Solar Wind

David S. Tonoian[1], Xiao-Jia Zhang[1,2], Anton Artemyev[2], Qianli Ma[3,4], Robert W. Ebert[5,6], and Frederic Allegrini[5,6]

[1]Department of Physics, University of Texas at Dallas, Richardson, TX, USA, [2]Department of Earth, Planetary, and Space Sciences, University of California, Los Angeles, CA, USA, [3]Department of Atmospheric and Oceanic Sciences, University of California, Los Angeles, CA, USA, [4]Center for Space Physics, Boston University, Boston, MA, USA, [5]Southwest Research Institute, San Antonio, TX, USA, [6]Department of Physics and Astronomy, University of Texas at San Antonio, San Antonio, TX, USA

Key Points:

- We compare kinetic, thermal, and magnetic field energies of current sheets in solar wind and in magnetospheres of Earth, Mars, and Jupiter
- Parameter regimes of current sheets in Martian magnetotail overlap with those found in solar wind, Earth's magnetosheath and magnetotail
- Current sheets in the Jovian magnetotail display unique parameter regimes not observed in the near-Earth plasma environment

Supporting Information:

Supporting Information may be found in the online version of this article.

Correspondence to:

D. S. Tonoian,
david.tonoian@utdallas.edu

Citation:

Tonoian, D. S., Zhang, X.-J., Artemyev, A., Ma, Q., Ebert, R. W., & Allegrini, F. (2025). Parametric regimes of thin current sheets in planetary magnetospheres and solar wind. *Journal of Geophysical Research: Space Physics*, *130*, e2025JA033942. https://doi.org/10.1029/2025JA033942

Received 8 MAR 2025
Accepted 10 JUN 2025

Abstract Current sheets are quasi-1D layers of strong current density, which play a crucial role in storing magnetic field energy and subsequently releasing it through charged particle acceleration and plasma heating. They are observed in planetary magnetospheres and solar wind flows, where they are also known as solar wind discontinuities. Despite significant variations in plasma parameters across different magnetospheres and the solar wind, current sheet configurations can remain fundamentally similar. In this study, we analyze current sheets observed in various regions, including the near-Earth (within 30 Earth radii) and distant (50–200 Earth radii) magnetotail, Earth's dayside and nightside magnetosheath, the near-Earth solar wind, and Martian and Jovian magnetotails. We examine three key plasma parameters: the plasma beta (ratio of plasma to magnetic pressure), the Alfvénic Mach number (ratio of plasma bulk flow speed to Alfvén speed in the current sheet reference frame), and the ion to electron temperature ratio. Additionally, we investigate the kinetic, thermal, and magnetic field energy densities. Our cross-system analysis demonstrates that the same current sheet configuration can exist across a very wide parametric space spanning multiple orders of magnitude. We also highlight the distinct plasma environments of the Martian and Jovian magnetotails, characterized by large populations of heavy ions, emphasizing their significance in comparative magnetospheric studies.

1. Introduction

Current sheets are spatially localized, quasi-1D layers of strong electric currents that naturally form in plasma systems of various magnetic field configurations (Parker, 1994; Priest, 1985; Syrovatskii, 1981). They serve as key sites for magnetic energy storage and release, driving fundamental processes such as magnetic reconnection (e.g., Lui, 2004; Pritchett & Coroniti, 2011; Sitnov et al., 2019; Zaitsev et al., 2025). Magnetic reconnection plays a crucial role in plasma heating and charged particle acceleration across space and astrophysical systems (Gershman et al., 2024; Gonzalez & Parker, 2016; Hoshino & Lyubarsky, 2012; Nakamura et al., 2024; Oka et al., 2023). While Earth's magnetosphere is our primary natural laboratory for investigating current sheet formation and dynamics (Angelopoulos, McFadden, et al., 2008; Baker et al., 1996; Sitnov et al., 2019), similar processes are believed to be important in the solar corona (e.g., Aschwanden, 2002; Pezzi et al., 2021; Zharkova et al., 2011), the solar wind (Gosling, 2012; Khabarova et al., 2021; Phan et al., 2006, 2020), and various astrophysical systems (e.g., Arons, 2012; Cerutti et al., 2014; Guo et al., 2024). Understanding the parametric regimes that govern current sheet formation is therefore crucial for advancing our knowledge of magnetic reconnection in diverse plasma environments.

Earth's magnetosphere provides an ideal setting for current sheet investigations (see discussion in An et al., 2023). In the near-Earth magnetotail, thin and intense current sheets are primarily supported by hot protons (Petrukovich et al., 2015), with currents predominantly driven by proton diamagnetic drifts and cross-field flows (see A. V. Artemyev, Petrukovich, et al., 2011; Runov et al., 2006). In the more distant magnetotail, around and beyond the lunar orbit, colder plasma and fast flows (almost reaching the supersonic limit) (Hoshino et al., 2000; Walia et al., 2024) give rise to current sheets resembling slow shock waves (A. V. Artemyev, Angelopoulos, Runov, & Vasko, 2017; Hietala et al., 2015; Hoshino et al., 1996). Due to weak plasma pressure contributions, these distant magnetotail current sheets often adopt a so-called force-free configuration (see review by Neukirch, Wilson, and Allanson (2020)), where field-aligned currents play a dominant role (Kamaletdinov et al., 2024b; Xu et al., 2018), similar to those observed at the magnetopause (e.g., Panov et al., 2011; A. S. Lukin et al., 2020).

Outside the magnetopause, in the magnetosheath, subsonic plasma flows on the dayside can be accelerated (via the magnetic tension force; see A. V. Artemyev et al., 2022; S.-H. Chen et al., 1993; Erkaev et al., 2011) to the supersonic regime in the nightside, distant magnetosheath. These flows often contain multiple embedded current sheets (discontinuities), which either emerge from local magnetic field turbulence (e.g., Chaston et al., 2020; C. H. K. Chen & Boldyrev, 2017; Sahraoui et al., 2006) or are advected from the solar wind (Kropotina et al., 2021; Y. Y. Liu et al., 2022; A. Lukin et al., 2024). While predominantly force-free and ion-scale (although electron-scale current sheets can also be observed in the magnetosheath; see Phan et al., 2018), magnetosheath current sheets differ from those in the solar wind due to their higher ion plasma β (ratio of thermal to magnetic pressures). In the near-Earth solar wind, ion-scale current sheets (discontinuities) are quite widespread, with an occurrence rate exceeding one intense event per hour (Vasko et al., 2022; Vasquez et al., 2007). These current sheets are force-free and primarily supported by field-aligned currents (A. V. Artemyev, Angelopoulos, Vasko, Runov, et al., 2019; Vasko et al., 2022). These current sheets in the solar wind are unique in that the electron-to-ion temperature ratio, T_e/T_i, often exceed one (A. V. Artemyev, Angelopoulos, & Vasko, 2019; L. B. Wilson et al., 2018), unlike those in Earth's magnetosheath and magnetosphere, where ions remain significantly hotter than electrons (A. V. Artemyev, Baumjohann, et al., 2011; C.-P. Wang et al., 2012).

Despite the diversity in plasma β and electron-to-ion temperate ratios, the near-Earth plasma environment is characterized by low plasma density (n_p), high temperature (T_p), and is predominantly proton-dominated. The relatively high temperature leads to thermal effects dominating current sheet configurations, where the proton gyroradius ($\rho_p = v_{th}/\Omega_{cp} \propto \sqrt{T_p}$) exceeds the proton inertial length ($d_p = c/\omega_{pp} \propto 1/\sqrt{n_p}$), except in the solar wind where $\rho_p/d_p = \sqrt{\beta}$ can fall below one (Vasko et al., 2022). Therefore, to extend the range of observed current sheet regimes to low-β plasma ($\beta < 1$), we examine the Martian magnetotail, where dense, cold plasma dominates (e.g., Dubinin & Fraenz, 2015), and the Jovian magnetotail, where plasma is significantly more rarefied than in Earth's magnetotail (e.g., Huscher et al., 2021; Z. Y. Liu et al., 2024; J.-Z. Wang, Bagenal, Wilson, Valek, et al., 2024). Both magnetotails feature current sheets with $\rho_p/d_p < 1$ (observations, statistics for Mars, and observations for Jupiter, correspondingly A. V. Artemyev et al., 2023; A. V. Artemyev, Angelopoulos, Halekas, et al., 2017; Grigorenko et al., 2022). Moreover, these magnetotails are characterized by a high abundance of heavy ions: atomic and molecular oxygen ions in Martian current sheets (e.g., A. V. Artemyev, Angelopoulos, Halekas, et al., 2017), and sulfur and oxygen ions in Jovian current sheets (e.g., J.-Z. Wang, Bagenal, Wilson, Nerney, et al., 2024). In contrast, Earth's magnetotail remains proton-dominated, with heavy ion contributions—such as oxygen—being insufficient to significantly alter current sheet properties (e.g., Kistler et al., 2005; Mouikis et al., 2010; Petrukovich et al., 2015). The same holds true for helium ions in the solar wind (L. B. Wilson et al., 2018).

In this study, we compare parametric regimes of current sheets across different plasma environments, including the near-Earth solar wind, day- and nightside magnetosheath, near-Earth and distant magnetotail, and the magnetotails of Mars and Jupiter. We focus on dimensionless parameters (plasma beta, Alfvénic Mach number, and electron-to-ion temperature ratio) and dimensional energy densities (plasma flow, thermal, and magnetic field energy per particle). While individual plasma systems exhibit distinct current sheet characteristics, our cross-system analysis reveals well-organized trends between different energy components. We discuss these trends and compare the parametric regimes of current sheets in Earth's space environment with those in the Martian and Jovian magnetotails, offering new insights into the universal properties of current sheets in space plasmas.

2. Data Set and Instruments

In this study, we use two main data sets for each spacecraft mission: magnetic field vector **B** measured by flux gate magnetometers and plasma moments measured by electrostatic analyzers. Specifically, we use number density, velocity, temperature and thermal pressure for electrons (n_e, v_e, T_e, $p_e = n_e k_B T_e$, respectively, with k_B being the Boltzmann constant) and for each ion species that can be separated by the instrument (n_i, v_i, T_i, $p_i = n_i k_B T_i$, $i = \{H^+, \dots\}$).

For each data set, we use electron and ion moments along with magnetic field measurements to calculate plasma parameters inside current sheets. To define the current sheet region, we use a local coordinate system derived from the Minimum Variance Analysis applied to magnetic field (MVAB method, Sonnerup & Scheible, 2000). In this coordinate system, the unit vector **l** describes the direction of the most varying component of the magnetic field

and lies approximately within the current sheet plane, while the unit vector **n** is approximately normal to the current sheet. The third unit vector, **m**, completes the right-handed coordinate system (**l**, **m**, **n**). In this reference frame, we examine the region where the most varying magnetic field component, $B_l = (\mathbf{B}\cdot\mathbf{l})$, satisfies $|B_l| < (\max B_l - \min B_l)/4$, unless otherwise specified. In this region we determine the ion Alfvénic Mach number, $M_A = \langle v_{\Sigma i}\rangle / v_A$, where $\langle v_{\Sigma i}\rangle = \left\langle \left| \sum_i \mathbf{v}_i n_i / n_{\Sigma i} \right| \right\rangle$, the summation extends over all ion species, $n_{\Sigma i} = \sum_i n_i$ represents the total ion number density, and $v_A = \langle |\mathbf{B}| \rangle / \sqrt{\langle \sum_i m_i n_i \rangle \mu_0}$ is Alfvén velocity, with m_i denoting the ion mass. The averaging, $\langle \ldots \rangle$, applies to measurements taken within the sheet, where $|B_l| < (\max B_l - \min B_l)/4$ (for the exception of solar wind and magnetosheath data sets, see corresponding subsections). In addition, we calculate the ion bulk flow (kinetic) energy in the current sheet plane for each ion species, $K_i = m_i \langle v_{i,l}^2 + v_{i,m}^2 \rangle / 2$ for planetary magnetotails and $K_i = m_i v_{CS}/2$ for magnetosheath and solar wind current sheets (see definition of v_{CS} in Section 2.3). We also calculate the plasma beta, $\beta = \left(\sum_i p_i + p_e\right) / \left(B^2/2\mu_0\right)$, and estimate the characteristic value, $\beta_{\max}$, as the average of the top 10% highest values throughout the sheet. Further details, including the definition of the *inside* region of the current sheet and the ion species included in the calculations, are provided for each data set below.

There are two key assumptions underlying current sheet configurations. First, we assume that current sheets are quasi-one-dimensional structures, with the primary plasma and magnetic field gradients oriented across the current sheet surface, that is, along the normal vector **n**. This assumption is well-supported by observations in the solar wind (R. Wang et al., 2024), and has also been verified in the Earth's (e.g., A. V. Artemyev et al., 2015) and Jovian (e.g., A. V. Artemyev et al., 2014) magnetotails. For the Martian magnetotail, numerical simulations suggest that this assumption holds as well, as they show stretched magnetic field lines on the nightside (e.g., Quartey & Liemohn, 2025, and references therein). Second, we assume that current sheets are approximately balanced across their surface, following the relation $\nabla_n \left(B_l^2 + B_m^2\right) \approx 8\pi \nabla_n \left(\sum_i p_i + p_e\right)$. This balance has been confirmed by spacecraft measurements in both the Earth's magnetotail (e.g., Petrukovich et al., 1999) and the solar wind (e.g., A. V. Artemyev, Angelopoulos, & Vasko, 2019). It is important to note, however, that current sheets may not be fully balanced along the **l** direction (see discussion of this balance in Sitnov and Merkin (2016), Sitnov and Arnold (2025), A. V. Artemyev et al. (2021)). This aspect is not addressed in this study, as single-spacecraft observations do not allow for verification of longitudinal balance.

2.1. THEMIS Magnetotail Observations (2009)

The first data set comprises quiet-time magnetotail current sheets observed by THEMIS B, C, D and E spacecraft in January-March 2009. It includes 232 events spanning distances from 9 R_E to 35 R_E (R_E is the Earth radius) down tail (see details in A. V. Artemyev, Angelopoulos, and Runov (2016)). We use magnetic field data with spin resolution (~3 sec) from the Fluxgate Magnetometer (FGM) (Auster et al., 2008). Electron and ion moments are calculated from the combined fluxes of Electrostatic Analyzer (ESA) (McFadden et al., 2008) and Solid State Telescope (SST) (Angelopoulos, Sibeck, et al., 2008). All ion parameters are calculated by assuming a proton-electron plasma, as oxygen heavy ions do not significantly contribute to plasma moments in magnetotail current sheets (see discussion in A. V. Artemyev et al. (2009) and Petrukovich et al. (2015)).

2.2. ARTEMIS Magnetotail Observations (2010)

The second data set consists of Earth's distant magnetotail observations collected by ARTEMIS P1 and P2 spacecraft during their trans-lunar injection phase (March-September 2010). It includes 393 events spanning distances from 65 R_E to 170 R_E downtail (see discussion in A. V. Artemyev, Angelopoulos, Runov, and Vasko (2017)). Most events observed by P1 are located near the lunar orbit, closer to the end of the injection. The methodology for magnetic field sampling and moment calculations are the same as in the THEMIS magnetotail data set. However, only full-mode moments (~1 min time resolution) were available at that time. To improve temporal resolution, we estimate number density and ion and electron temperatures using the omnidirectional phase space density measurements from ESA's reduced mode (~3−4 sec resolution). Number density is integrated from phase space density and cross-validated with lower-time-resolution values calculated from full distribution onboard ARTEMIS (McFadden et al., 2008). Ion and electron temperatures are calculated as the second central moments of the phase space density, with electron temperature adjusted by removing the energy range below the spacecraft potential to mitigate photoelectron contamination.

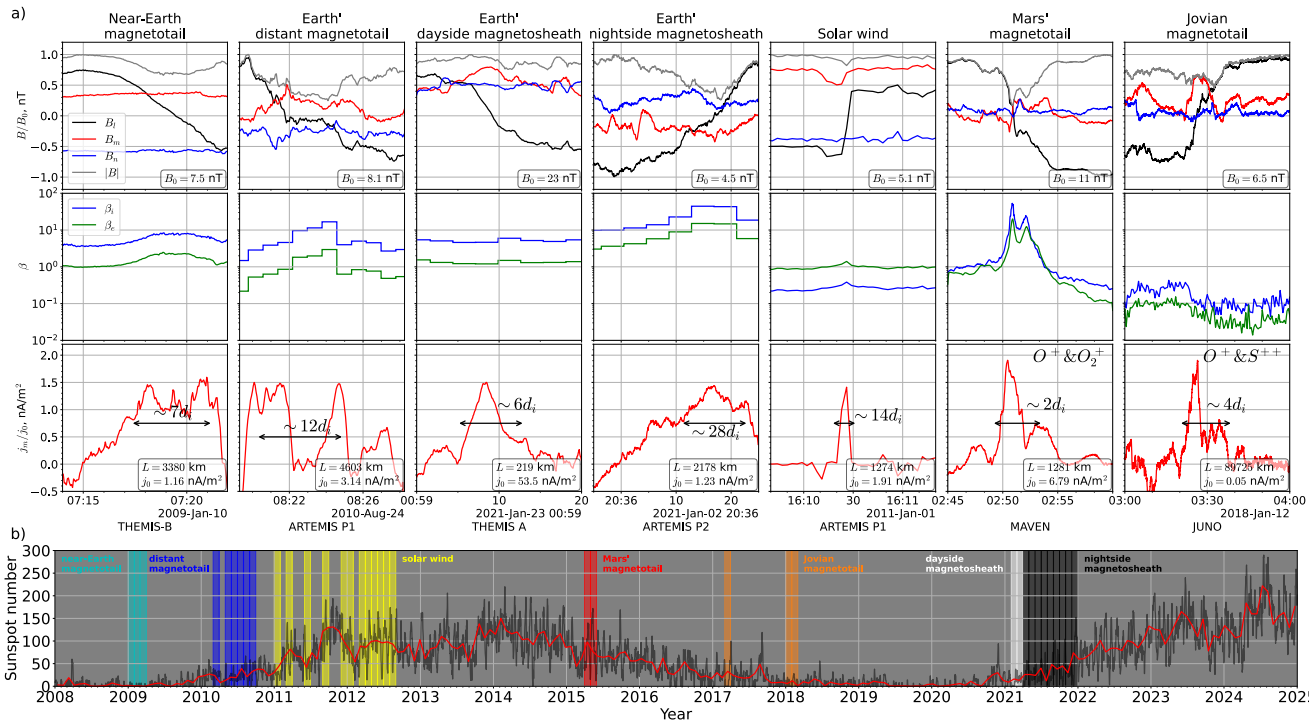

Figure 1. (a) Example current sheets from all regions analyzed in this study. The upper panels show the magnetic field components in the coordinate system of the current sheet (see text for details); the middle panels show ion and electron beta measurements across the current sheets; the lower panels show plasma current estimates, $j_m = -(dB_l/dt)/v_n\mu_0$ across the current sheets, along with spatial scale estimates (L) based on current sheet flapping motion (Hoshino et al., 1996; Sergeev et al., 1998; Vasko et al., 2015). The ion inertial length, $d_i = c/\omega_{pi}$, is calculated for the dominant ion species: protons for Earth's space environment, O_2^+ for the Martian magnetotail, and S^{++} for the Jovian magnetotail. For solar wind and magnetosheath events, plasma flow speed is used to estimate the spatial scale (see text for details). In the Jovian magnetotail, the spatial scale is estimated using the flapping motion speed asymptotic: $L = 225\ \text{km} \cdot \tan(9.5°) \cdot (\Delta t/1\ \text{sec})$ (Kim et al., 2020b). (b) Months coverage for each data set (color-filled areas) over daily (black line) and monthly averaged (red line) sunspot numbers (Clette & Lefèvre, 2015).

2.3. THEMIS Dayside Magnetosheath Observations

The dayside magnetosheath data set consists of ~100 current sheet events observed by THEMIS-A spacecraft in February–March 2021. As these current sheets have considerably smaller spatial scales (see one example from Figure 1), we use high-resolution magnetic field data (~0.25 seconds sampling rate) and restricted the data set to events where plasma moments exist both inside and around the current sheet crossing intervals (>6 sec). Due to the high bulk flow velocity in the magnetosheath and solar wind, current sheets are transported across spacecraft by these plasma flows, and estimation of normal to the current sheet could be very unreliable (R. Wang et al., 2024). We estimate the plasma velocity in the reference frame of the current sheet, assuming that the current sheet behaves as a rotational discontinuity (see discussion in A. V. Artemyev, Angelopoulos, and Vasko (2019) and Shen et al. (2024)). Under this assumption, we estimate the ion velocity in the reference frame of the current sheet as the variation in ion velocity along the most varying magnetic field component B_l (determined via the MVAB method): $v_{CS} = \max(\mathbf{v}\cdot\mathbf{l}) - \min(\mathbf{v}\cdot\mathbf{l})$. Note, because in solar wind current sheets the plasma parameters may vary from boundary to boundary, without symmetrical maximum/minimum relative to the current sheet center (see, e.g., A. V. Artemyev, Angelopoulos, & Vasko, 2019), averaging $\langle\ldots\rangle$ is considered across the entire current sheet region where $|B_l| < (\max B_l - \min B_l)$.

2.4. ARTEMIS Nightside Magnetosheath Observations

This data set for the nightside magnetosheath includes ~100 events during ARTEMIS spacecrafts magnetosheath crossings near the lunar orbit in May–December 2021. The data source and processing approach are the same as that used for the dayside magnetosheath observations.

2.5. ARTEMIS Solar Wind Observations

This final Earth-based data set includes 527 current sheet events captured by ARTEMIS spacecraft in the solar wind near lunar orbit during 2011–2012 (see details in A. V. Artemyev, Angelopoulos, & Vasko, 2019). Spin-resolution magnetic field data (∼4 s at the time) and plasma moments are used. Since ESA is not optimized for measuring cold solar wind ions, the ion temperature T_i is reconstructed based on its correlation with 1-min OMNI data (King & Papitashvili, 2005). Details of this reconstruction technique can be found in A. V. Artemyev et al. (2018).

2.6. Martian Magnetotail Observations

For Martian magnetotail current sheet crossings, we analyze 2 months of MAVEN observations (April and May 2015), with a total of 200 events (see details in A. V. Artemyev, Angelopoulos, Halekas, et al., 2017). During this period, MAVEN traversed the magnetotail at distances up to $3R_M$ (R_M is the radius of Mars). We use magnetometer (MAG) data (Connerney, Espley, DiBraccio, et al., 2015; Connerney, Espley, Lawton, et al., 2015) with a 1-s time resolution. Ion moments are obtained from the Suprathermal And Thermal Ion Composition (STATIC) sensor (McFadden et al., 2015), which distinguishes ion species with a 15-s time resolution. Electron moments come from the Solar Wind Electron Analyzer (SWEA) (Mitchell et al., 2016) with a 2-s time resolution. Due to spacecraft potential effects, estimating the electron density (n_e) can be challenging. Thus we use the total density sum of all ion species, $i = \{H^+, H_2^+, He^+, O^+, O_2^+\}$. The electron temperature is estimated using the electron thermal pressure relation, $T_e = p_e/n_{\Sigma i}$. Apart from these considerations, plasma parameter calculations are similar to those in the THEMIS/ARTEMIS data sets.

2.7. Jovian Magnetotail Observations

To compile a statistical data set of current sheets in the Jovian magnetotail, we examine Juno's 4*th*, 5*th*, 10*th* and 11*th* orbits (January–April 2017 and January–February 2018) (Bagenal et al., 2017), during which the spacecraft crossed the current sheet at distances of $30R_J$ to $105R_J$ (R_J is the Jovian radius) at the nightside to dawn sector (MLT 3–6) (see details in Z. Y. Liu et al. (2021, 2024)). This data set includes 47 events. We use the fluxgate magnetometer (MAG) data (Connerney, Adriani, et al., 2017; Connerney, Benn, et al., 2017) in the sun-state coordinate system with a 1-s sampling rate. Electron and ion moments are obtained from the Jovian Auroral Distributions Experiment (JADE) (McComas, Alexander, et al., 2017; McComas, Szalay, et al., 2017), following the methodology described in Kim et al. (2020a, 2020b). JADE differentiates ion species, and we use proton and heavy ion moments. For heavy ions, we assume the dominant contribution comes from equal mix of O^+ and S^{++} ions (see details in Kim et al., 2020b; J.-Z. Wang, Bagenal, Wilson, Valek, et al., 2024).

3. Comparison of Current Sheet Parametric Regimes

3.1. $M_A - \beta$ Parametric Space

Figure 2a shows the parametric domains occupied by current sheets within the $(M_A, \beta_{\max})$ space. Contours of magnetosonic Mach number are also plotted, $M = M_A/\sqrt{1 + \gamma\beta_{\max}/2}$ ($\gamma = 5/3$, Goertz & Baumjohann, 1991). Solar wind current sheets (discontinuities; yellow region) are observed in low-β (with $\beta_{\max} \in [0.5, 20]$) and mostly sub-Alfvénic (with $M_A < 1$) regimes (note that we examine plasma flows in the discontinuity reference frame, with the solar wind bulk flow removed). Due to the low β, even sub-Alfvénic conditions may be close to super-sonic, and when M_A reaches one, M approaches one.

As solar wind current sheets traverse the dayside bow shock and penetrate into the dayside magnetosheath (white region), thermalization of solar wind flows significantly increases plasma β, with $\beta_{\max} \in [2, 180]$. The plasma flow speed in the current sheet reference frame remains largely unchanged, $M_A < 2$ and $M < 1$. Similar conditions are observed in the nightside distant magnetosheath (black region), but with the decrease on upper bound of $\beta_{\max} \in [2, 60]$ and slight increase in Alfveénic Mach number, although still in $M < 1$,indicating that plasma flow acceleration (e.g., Erkaev et al., 2011; Harris et al., 2013) and adiabatic cooling (e.g., A. V. Artemyev et al., 2022) do not significantly change the parametric space of current sheets.

As plasma from the distant magnetosheath crosses the flank magnetopause, it fully thermalizes and fills the distant magnetotail (e.g., Hasegawa, 2012; A. S. Lukin et al., 2020). Consequently, current sheets observed in the

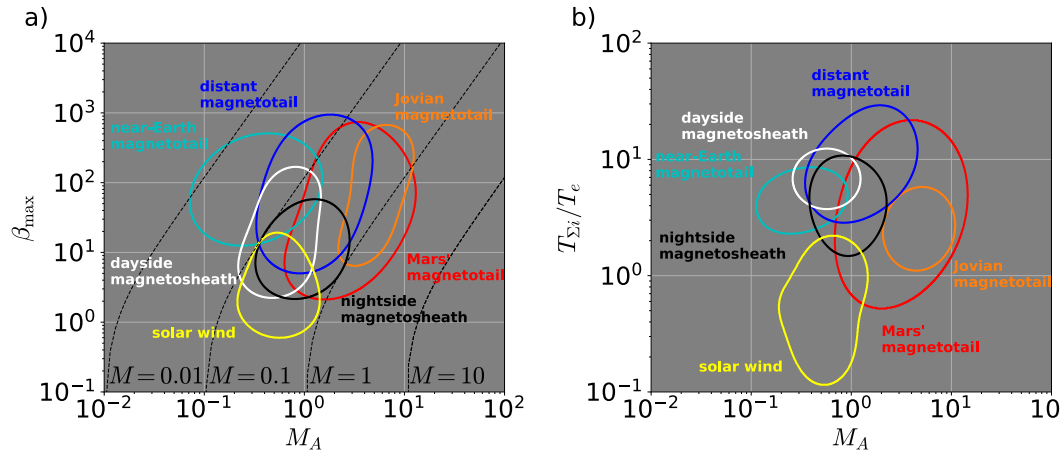

Figure 2. Distributions of plasma parameters for all current sheet data sets in (a) $\beta_{\max} - M_A$ and (b) $T_i/T_e - M_A$ space. Each contour represents the region where ~80% of the events are located. Dashed lines in panel (a) represent levels of Mach number $M = \langle v_i \rangle / c_{ms}$, where $c_{ms} = v_A\sqrt{1 + (5/6)\cdot\beta}$ is the magnetosonic speed. Ion speed is estimated in the reference frame of the current sheet. Contours are defined using One-Class Support Vector Machine with Gaussian Radius Basis Function kernel (for derivation and application see Schölkopf et al., 2001). Scatterplots for these and following figures with all events are provided in Supporting Information S1.

distant magnetotail (dark blue region) exhibit higher $\beta_{\max} \in [5, 1000]$. Such high-$\beta$ environments are associated with strong (intense) diamagnetic currents, which are unstable to magnetic reconnection (see review by Gonzalez and Parker (2016)). Indeed, the distant magnetotail hosts fast plasma flows reaching $M \sim 1$ (see also Hietala et al., 2015; Hoshino et al., 2000; Walia et al., 2024). Solar wind, day- and nightside magnetosheath, and distant magnetotail current sheets collectively exhibit a trend within the $(M_A, \beta_{\max})$ space: their parametric regions align with the $M \sim 1$ boundary and extend toward higher M_A as $\beta_{\max}$ increases. This suggests that $M \sim 1$ acts as a natural limit for fast plasma flows; beyond this threshold ($M > 1$), flow instabilities may disrupt current sheets (see discussion in Hoshino and Higashimori (2015), Shi et al. (2021), and Shi (2022)). However, due to the prevalence of current sheets in stagnant plasma ($M_A < 1$), this trend becomes apparent only when examining multiple regions (from solar wind to the distant magnetotail) together.

In the near-Earth magnetotail, proton temperatures are significantly higher (~10 keV) (A. V. Artemyev, Baumjohann, et al., 2011; C.-P. Wang et al., 2012) than in the distant magnetotail (just a thermalized solar wind flow with the thermal energy ~1 keV; see A. V. Artemyev, Angelopoulos, Runov, Wang, & Zelenyi, 2017; A. S. Lukin et al., 2020). This hot plasma environment inhibits the formation of reconnection-driven plasma flows with $M \sim 1$ (see An et al., 2022; Birn & Hesse, 2005, 2014; Lu et al., 2018, for details of energy conversion in the magnetotail magnetic reconnection), resulting in near-Earth current sheets (light blue) occupying a distinct parametric region. Note that the magnetic field is also stronger in the near-Earth magnetotail, reducing $\beta_{\max}$ compared to the distant tail.

Current sheets in the Jovian (orange region) and Martian (red region) magnetotails occupy a similar parametric domain to the Earth's distant magnetotail but extend across the $M = 1$ boundary. These current sheets form in high-β $(\beta_{\max} \in [2, 800])$ environments with fast plasma flows (high M).

In the Jovian magnetotail ($>30R_J$), plasma density is very low ($\sim[10^{-2}, 10^{-1}]$ cm^{-3}, see statistics in Huscher et al. (2021)), but a significant fraction consists of a mixture of oxygen ions O^+ and sulfur ions S^{++} with $m_i/q_i = 16m_p/e$ (see statistics in Kim et al. (2020b) and Z. Y. Liu et al. (2024)); that is, the mass density $m_i n > m_p \cdot 0.6$ cm^{-3} is comparable with that in Earth's magnetotail. The magnetic field is comparable to the Earth's distant magnetotail (~5–15 nT, see Z. Y. Liu et al., 2021). Therefore, reconnection-driven flows (~100–1000 km/s, see Kasahara et al., 2011; J.-Z. Wang, Bagenal, Wilson, Valek, et al., 2024) can be highly super-Alfvénic ($M_A > 10$ for some events) and even supersonic ($M > 1$). Although these conditions are more extreme than those in Earth's distant magnetotail, where $M \sim 1$ is rarely reached (e.g., Hoshino et al., 2000; Walia et al., 2024), the magnetic field configuration of Jovian magnetotail current sheets closely resembles that of Earth's magnetotail. In both systems, the magnetic field gradients (across the current sheet, $\nabla_n B_l^2$, and along the

current sheet, $B_n\nabla_n B_l$) for the majority of current sheets are balanced by plasma (ion) pressure gradients ($\nabla_n p_i$ and $\nabla_l p_i$), while a subset of force-free current sheets with $\nabla_n B_l^2 \approx \nabla_n - B_m^2$ and $\nabla_n p_i \approx 0$ is also observed (A. V. Artemyev et al., 2014; Kamaletdinov et al., 2024b).

In the Martian magnetotail, plasma density is significantly higher ($\sim$10–100 cm^{-3}, see in Dubinin et al., 2011; Inui et al., 2018), and ion composition is dominated by ionized oxygen atoms with $m_O/m_p = 16$ and molecular ions with $m_{O2}/m_p = 32$ (Carlsson et al., 2006; Maes et al., 2021). These ions are of ionospheric origin with low temperature (<1 keV; see Fedorov et al., 2006; Dubinin et al., 2013; Harada et al., 2015). The magnetic field ($\sim$5–15 nT, see A. V. Artemyev, Angelopoulos, Halekas, et al., 2017; Grigorenko et al., 2019; Zhang et al., 2023) is comparable to the Earth's distant magnetotail. Therefore, the Alfvén speed and magnetosonic speed in the Martian magnetotail are significantly lower than those in Earth's magnetotail, whereas the plasma flow velocities in these two systems are comparable, $\geq$100 km/s (e.g., Dubinin et al., 2011; Harada et al., 2015, 2020). Therefore, current sheets in the Martian magnetotail can form in super-Alfvenic (M_A reaching 10) and supersonic ($M > 1$) plasma. Despite these differences in plasma parameters, the configuration of current sheets in the Martian magnetotail closely resembles that observed in Earth's distant magnetotail, with both pressure-balanced and force-free current sheets present (A. V. Artemyev, Angelopoulos, Halekas, et al., 2017; DiBraccio et al., 2015; Grigorenko et al., 2022; Li et al., 2023). The main difference is that in the Martian magnetotail, electrons contribute comparably (with ions) to the pressure balance, because hot solar wind electrons ($\sim$100 eV) have a temperature comparable to cold ionospheric ions (see discussion below).

3.2. $M_A - T_i/T_e$ Parametric Space

Figure 2b shows the parametric regime of current sheets in $\left(M_A, T_{\sum i}/T_e\right)$ space, where $T_{\sum i}$ is the average ion temperature. This differs from the proton temperature only in MAVEN and Juno observations, as the electrostatic analyzer onboard THEMIS/ARTEMIS does not distinguish between ion species. For current sheets in slow plasma flows ($M_A < 1$), the temperature ratio primarily determines the dominant contributor to thermal plasma pressure in the stress balance. In contrast, for current sheets associated with fast flows ($M_A \geq 1$), this ratio provides insight into the redistribution of flow energy between ions and electrons in flow-generating regions (e.g., reconnection region; see discussion in Phan et al. (2014) and Øieroset et al. (2024)).

In current sheets (discontinuities) observed in the solar wind (yellow region), electron temperatures can be significantly higher than proton temperatures (see statistics for solar wind plasma in L. B. Wilson et al. (2018)). These current sheets are either balanced by plasma flows ($M_A \sim 1$), as in Alfvénic-type rotational discontinuities (e.g., A. V. Artemyev, Angelopoulos, Vasko, Runov, et al., 2019; De Keyser & Roth, 1998; Vasquez & Hollweg, 2001), or by thermal pressure gradients ($M_A < 1$), as in tangential discontinuities (e.g.,Neukirch, Vasko, et al., 2020; Neukirch, Wilson, & Allanson, 2020). In the latter case, electrons likely dominate the pressure balance.

Except for the solar wind, the only plasma system having substantial population of current sheets with $T_{\sum i}/T_e \sim 1$ is the Martian magnetotail (red region). Here, hot solar wind electrons may mix with cold ionospheric ions, both with thermal energies around $\sim$100eV (e.g., Curry et al., 2022; DiBraccio et al., 2015). This cold plasma background favors the formation of force-free current sheets balanced by plasma flow gradients (see discussion in An et al., 2023). Indeed, MAVEN observations confirm the presence of force-free current sheets in the Martian magnetotail (A. V. Artemyev, Angelopoulos, Halekas, et al., 2017), with properties similar to those of solar wind discontinuities.

As the solar wind crosses the bow shock, plasma thermalization significantly increases ion temperature, leading to $T_{\sum i}/T_e > 1$ (white and black regions of dayside and nightside magnetosheath). Further ion heating due to plasma flow thermalization at the magnetopause in the distant tail (A. V. Artemyev, Angelopoulos, Runov, Wang, & Zelenyi, 2017; A. S. Lukin et al., 2020) results in $T_{\sum i}/T_e \sim 10$ for current sheets detected there (blue region). Here, plasma flows—likely due to distant magnetic reconnection—can be quite fast, reaching $M_A > 1$. Interestingly, observations in the Martian magnetotail (red region) span all parametric regimes, from $T_{\sum i}/T_e < 1$ (solar wind-like) to $T_{\sum i}/T_e \sim 3$ (magnetosheath-like), and up to $T_{\sum i}/T_e \sim 10$ (distant magnetotail-like). This variability makes Martian magnetotail a unique system for investigating current sheet configurations.

The Jovian magnetotail (orange region) and near-Earth magnetotail (light blue region) exhibit relatively hot electrons, with $T_{\sum i}/T_e \in [2,8]$. However, these two systems differ significantly in plasma flow speeds: in the near-Earth magnetotail, strong magnetic field and weak plasma flows result in $M_A < 1$, whereas in the Jovian magnetotail, the presence of heavy ions lowers the Alfvén speed, allowing the plasma flows to become super-Alfvénic ($M_A > 1$). The mechanisms of electron heating in these two plasma systems are also distinct. In the near-Earth magnetotail, current sheets form in electron populations transported from the distant tail and heated by the convection electric field (see A. V. Artemyev et al., 2012; Shustov et al., 2021). This heating is more effective for electrons than for ions, causing $T_{\sum i}/T_e$ to decrease with decreasing radial distance from Earth (see C.-P. Wang et al., 2012). In contrast, in the Jovian magnetotail, ion and electron temperatures remain relatively constant with radial distance (Z. Y. Liu et al., 2024), as hot ions and electrons originate in the inner magnetosphere and are transported tailward without significant energy change (see discussion in Jackman et al., 2014; Krupp et al., 2015).

Overall, Figure 2b demonstrates that the Earth's space environment spans a broad range of $T_{\sum i}/T_e \in \left[10^{-1}, 4\cdot 10^{2}\right]$, with M_A primarily around/below one. A similarly wide range of $T_{\sum i}/T_e$ is observed in the Martian magnetotail, suggesting that current sheets in this system can exhibit pressure balance configurations resembling those found in the solar wind, magnetosheath, and distant magnetotail. Meanwhile, current sheets in the near-Earth magnetotail resemble those in the Jovian magnetotail in $T_{\sum i}/T_e$, but the latter features much faster plasma flows.

3.3. $K_i - T_i$ Parametric Space

Figure 2 shows the distribution of current sheets in the space of dimensionless system parameters. However, we also aim to investigate the ranges of different energy types accessible in Earth's space environment and compare them with those found in the Martian and Jovian magnetotails. We consider three types (forms) of energies associated with current sheet plasma and magnetic field dynamics (see An et al., 2022; Birn & Hesse, 2005; Eastwood et al., 2013; Lu et al., 2020): ion thermal energy (temperature), ion kinetic energy (K_i), and magnetic field energy per particle $\left(m_i v_{A,i}^2/2\right)$. Except for the second distribution for MAVEN, all data are shown for proton mass. Note, for most of the current sheets we cannot determine a local coordinate system accurately enough to consistently separate three components of the kinetic energy. Therefore, we consider K_i as a sum of $m_i v_{i,l}^2/2$ and $m_i v_{i,m}^2/2$, energy of plasma flows within the current sheet plane.

Figures 3a and 3c show distributions of current sheets in the (T_i, K_i) space and distributions of T_p/K_p. In the near-Earth solar wind, nearly half of observed current sheets have $K_p > T_p$ (main ion population), with majority distributed around $T_i \approx K_i$ within the [1,40]eV range. After thermalization at the bow shock, thermal energy increases significantly. In the dayside magnetosheath, current sheets exhibit $T_i > K_i$ with $T_i \in [100, 600]$ eV. Most likely the plasma adiabatic cooling occurs as the plasma propagates through the expanding magnetosheath toward the nightside (A. Artemyev et al., 2021, and references therein), resulting in $T_i \in [20, 200]$ eV for current sheets in the night-side magnetosheath, but still satisfying $T_i > K_i$ in the majority of events. Upon crossing the magnetopause, plasma flow is further thermalized, yielding $T_i \in [200, 3300]$ eV in the distant magnetotail. The large K_i in this region is associated with fast plasma flows from magnetic reconnection, where K_i may reach 1 keV, but observed current sheets almost never cross $T_i = K_i$ line, at best only reaching the slow shock regime (see discussion in Hoshino et al., 2000; Walia et al., 2024). Therefore, additional plasma heating in the distant magnetotail is likely associated with the thermalization of plasma flows from the magnetic reconnection region (see reviews by Pontin and Priest (2022); Y.-H. Liu et al. (2024), and references therein). Overall, current sheets in solar wind, day- and nightside magnetosheath, and distant magnetotail form a well-defined trend around the $T_i \approx K_i$ diagonal, spanning four orders of magnitude in T_i $\left(\left[1, 10^4\right]\text{ eV}\right)$.

A similar trend is observed in the MAVEN data set, where majority of current sheets distribute around $T_p \geq K_p$ and proton temperature falls in the range of $T_i \in [30, 1000]$ eV. In the Martian magnetotail, fast plasma flows arise from magnetic reconnection and magnetic field tension forces (see observations in Harada et al., 2015; DiBraccio et al., 2015; Harada et al., 2020). Thermalization of these flows likely contributes to the observed $T_i \approx K_i$ trend. Interestingly, for heavy ions, the kinetic energy, K_i, can even exceed thermal energy T_i (see red dashed contour), suggesting additional heating for heavy ions (mostly oxygen ions and ionized molecules) from

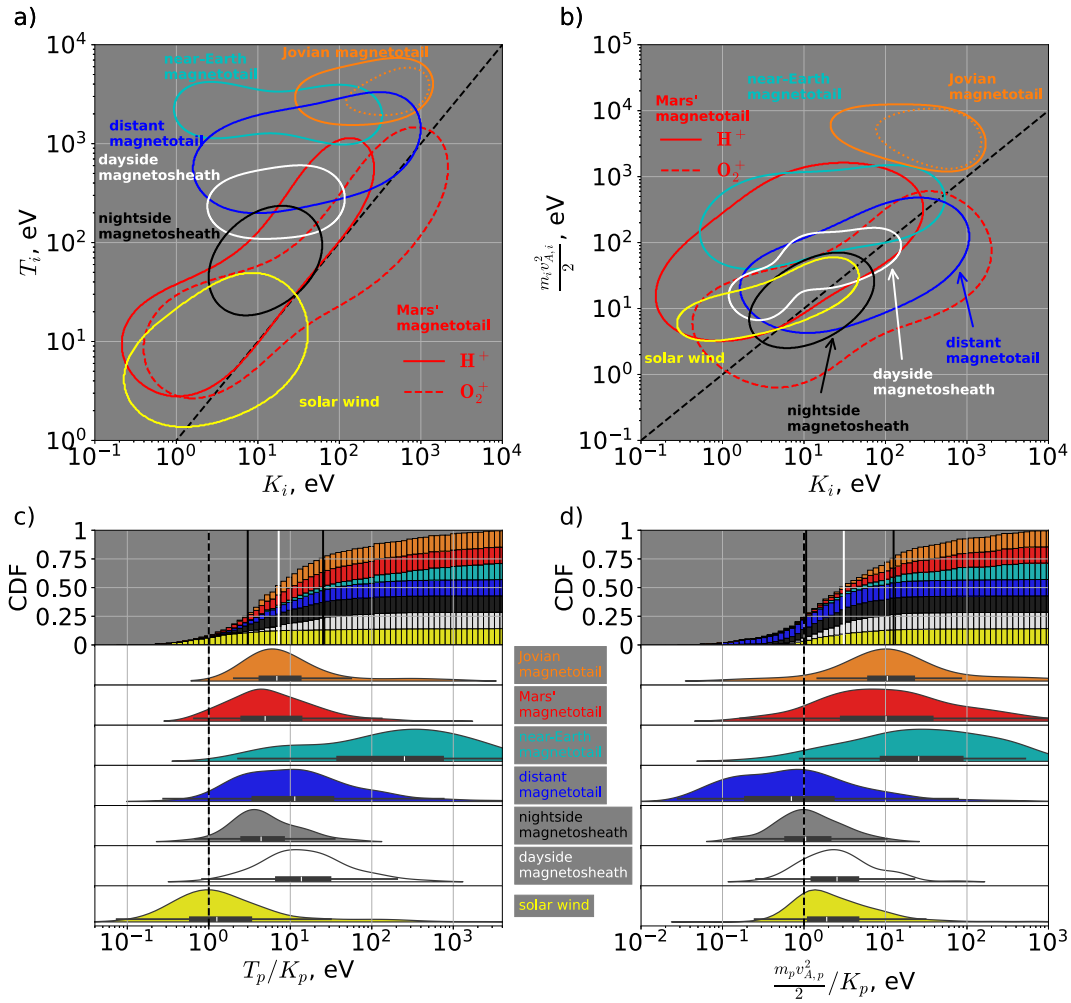

Figure 3. Distributions of plasma parameters for all data sets in panel (a) ion temperature T_i to ion bulk flow energy (per ion) K_i for protons (solid lines) and O_2^+ ions (for Mars' magnetotail, dashed line). (b) Magnetic field energy per ion $m_i v_{A,i}^2/2$ for protons and O_2^+ ions against the bulk flow energy K_i. Dotted orange lines for Jovian magnetotail in panels (a) and (b) mark 65% contours where core of the distribution is located. (c) and (d) Distributions of T_p/K_p and $(m_p v_{A,p}^2/2)/K_p$ (for protons) for each data set, box plots show first, third quartiles (in black) and median value (in white); top panels show total cumulative distribution function, each data set is normalized have equal value, solid black and white lines show first, third quartiles and median value; dashed lines show ratio $T_p = K_p$ and $m_p v_{A,p}^2/2 = K_p$.

magnetic reconnection (see discussion in Karimabadi et al., 2011; Liang et al., 2016). The domain of proton T_p and K_p for current sheets observed in the Jovian magnetotail (orange region) naturally extends the MAVEN domain to $T_i > 1$ keV, while maintaining the $T_i \geq K_i$ trend. Fast plasma flows in the Jovian magnetotail are similarly associated with magnetic reconnection (e.g., Kasahara et al., 2013), and their thermalization likely contributes to proton heating (see Z. Y. Liu et al., 2024; J.-Z. Wang, Bagenal, Wilson, Valek, et al., 2024, for the trend of proton temperature increase closer to Jupiter, where most of plasma flows are expected to break by the strong magnetic field).

In contrast, current sheets in the near-Earth magnetotail (light blue region) exhibit $T_i \gg K_i$, that is, thermalization of plasma flows no longer significantly heats protons. This results from efficient proton heating via plasma convection (from ~1 keV in the distant tail to ~5 keV in the near-Earth tail; see A. V. Artemyev, Angelopoulos, Hietala, et al., 2017), whereas the kinetic energy of plasma flows mostly remains below 1 keV within the magnetotail (see statistics in Kissinger et al., 2012; Juusola, Østgaard, & Tanskanen, 2011; Juusola, Østgaard, Tanskanen, Partamies, & Snekvik, 2011). In the near-Earth magnetotail, the fastest plasma flows occur after substorm onset, when thin current sheet breaks and the magnetic field dipolarizes (see reviews by Sitnov

et al. (2019) and Runov et al. (2021)); this explains why the statistics of thin current sheets in Figure 3a may not include the fastest flows with $K_i > 1$keV.

3.4. $K_i - m_i v_{A,i}^2/2$ Parametric Space

Figures 3b and 3d show current sheet observations in the $\left(K_i, m_i v_{A,i}^2/2\right)$ space and distributions of protons $\left(m_p v_{A,p}^2/2\right)/K_p$ ratio. The magnetic field energy per particle, $m_i v_{A,i}^2/2$, represents the energy available for particle acceleration in magnetic reconnection (see discussion in Phan et al. (2014), Barbhuiya et al. (2022), and Øieroset et al. (2024)). Some relation between K_i and $m_i v_{A,i}^2/2$ is thus expected. Indeed, all current sheet regions are clustered around the diagonal $K_i = m_i v_{A,i}^2/2$ (i.e., flow speed near the Alfvén speed). In the solar wind, dayside and nightside magnetosheath, and the Earth's distant magnetotail, current sheets exist within both sub-Alfvénic $\left(K_i < m_i v_{A,i}^2/2\right)$ and super-Alfvenic $\left(K_i > m_i v_{A,i}^2/2\right)$ flows. This implies that while magnetic reconnection contributes significantly to plasma kinetic energy, alternative plasma acceleration mechanisms also exist to result in $K_i > m_i v_{A,i}^2/2$ (e.g., magnetic field line tension force in the magnetosheath (A. Artemyev et al., 2021; Erkaev et al., 2011)). Comparison of Figures 3a and 3b shows that plasma flows generated by magnetic reconnection are thermalized, leading to proton heating following the classical energy conversion scenario: from magnetic field energy to plasma flows, and then to thermal energy (see reviews by Forbes, 2001; Kulsrud, 2001; Pontin & Priest, 2022; Y.-H. Liu et al., 2024).

In the near-Earth, Jovian, and Martian (for the protons) magnetotails, the available magnetic field energy exceeds plasma kinetic energy in majority of events $\left(K_p < m_p v_{A,p}^2/2\right)$. This confirms that in these plasma environments, magnetic reconnection transfers a portion of the magnetic field energy into plasma kinetic energy (plasma flows) (e.g., Øieroset et al., 2024; Phan et al., 2014), with no alternative acceleration mechanisms, keeping plasma flows consistently sub-Alfvénic. However, heavy ions observed in the Martian magnetotail (red dashed region) exhibit super-Alfvénic and (compare with panel (a)) likely super-sonic flows.

Overall, Figure 3 demonstrates that current sheets in various plasma systems adhere to expected trends: $T_i \gtrsim K_i$, $K_i \sim m_i v_{A,i}^2/2$. While these trends may be less apparent in individual plasma systems, they emerge clearly when plotted over a broad parametric range $(T_i, K_i, m_i v_{A,i}^2/2 \in \left[1, 10^4\right]$ eV). We can also confirm that by looking at distribution functions among all data sets on upper panels of Figures 3c and 3d, where each data set gives the same total contribution to the distribution function (weight of each event is inversely proportional to the length of the corresponding data set). Here we can see that third and first quartiles of such distributions lay within $T_p/K_p \in [2, 20]$ and $\left(m_p v_{A,p}^2/2\right)/K_p \in [1, 8]$.

3.5. $\rho_i - d_i$ Parametric Space

In the fluid stress balance equation, two key terms counteract the magnetic field tension: the inertial term $m_i n_i(\mathbf{v}\cdot\nabla)\mathbf{v}$ and pressure gradient term ∇P. For Alfvénic flows where $M_A \sim 1$, the ratio of these terms is $\beta_i = \rho_i^2/d_i^2$, where $d_i = c/\omega_{pi} = \sqrt{m_i c^2/4\pi e^2 n_i}$ is the ion inertial length and $\rho_i = v_{th}/\Omega_{ci} = \sqrt{2k_B T_i m_i c^2/e^2 B^2}$ is the ion gyroradius. In high-beta plasmas, the thermal pressure dominates the balance, making ρ_i the primary spatial scale; in contrast, the ion inertial length is the primary spatial scale in low-beta plasmas. The relationship between these scales follows a simple relation: $d_i/\rho_i = 1/\sqrt{\beta_i}$; but how are the parametric domains of observed current sheets structured in the $\left(d_i, \rho_i\right)$ space? We examine plasma systems spanning a wide range of β_i from $\sim 10^{-1}$ (typical of the solar wind and Martian magnetotail) to 10^2 (found in the Earth's distant magnetotail). Given this broad range, one might expect little correlation between d_i and ρ_i. Yet, Figure 4 demonstrates that current sheet are well organized within the $\left(d_i, \rho_i\right)$ space. Specifically, solar wind current sheets (yellow region) occupy the domain $d_i \sim 100$ km, $\rho_i \sim d_i/2$, showing a clear trend of increasing d_i with ρ_i increase for $\beta_i \in \left[10^{-1}, 2\right]$. Current sheets in dayside and nightside magnetosheath (white and black regions) reproduce the solar wind trend but for $\beta_i \in [2, 50]$, with $d_i \sim 50$ km and $\rho_i \sim d_i$. Martian magnetotail current sheets (red region) extend the solar wind and magnetosheath domains to $d_i \in [100, 1000]$ km and $\rho_i \in [50, 800]$ km. For heavy oxygen ions, this domain still shows a the same trend between d_i and ρ_i, but for $\beta_i \in \left[1, 10^2\right]$. The largest β_i are observed in the Earth's magnetotail (light blue and blue regions), where $d_i \in [300, 1000]$km and $\rho_i \in [700, 8000]$ km. Jovian magnetotail current sheets (orange regions) occupy an even larger domain, spanning $d_i \in [1000, 20000]$ km and

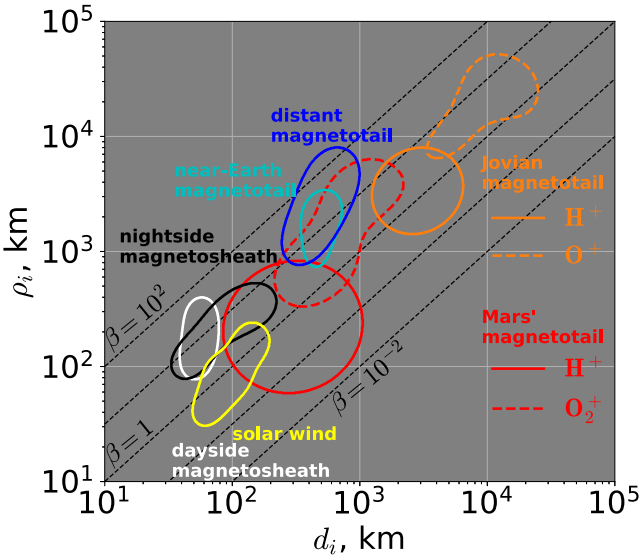

Figure 4. Distributions of plasma parameters for all data sets in the ion gyroradius ρ_i and ion inertial length d_i space. Solid lines represent proton-based parameter space, while dashed lines indicate data for the most abundant heavy ions (O_2^+ in Martian magnetotail, O^+ in the Jovian magnetotail).

$\rho_i \in [1000, 50000]$ km, while still maintaining similar range within $\beta_i = \rho_i^2/d_i^2 \in [10^{-1}, 10^2]$. Overall, Figure 4 demonstrates that the spatial scales of current sheets, governed by ion inertial and thermal pressure, exhibit a general trend of increasing d_i with ρ_i increase when analyzed over a sufficiently broad range. This suggests that Earth's space environment (including the distant tail) can replicate regimes of current sheets found in the Martian magnetotail (see also Figures 2 and 3). However, current sheets in the Jovian magnetotail appear more distinct in plasma parameters and are not mirrored in Earth's space environment.

4. Discussion and Conclusions

In this study, we provide a comparative analysis of current sheets observed in various space plasma environments, spanning three orders of magnitude in plasma β ($\in [1, 10^3]$), nearly three orders of magnitude in ion-to-electron temperature ratio ($T_i/T_e \in [10^{-1}, 50]$), two orders of magnitude in Alfvénic Mach number ($M_A \in [10^{-1}, 10^1]$), nearly four orders of magnitude in ion thermal energy ($T_i \in [1, 10^4]$ eV), at least three orders of magnitude in ion kinetic energy ($K_i \in [1, 10^3]$ eV), and four orders of magnitude in magnetic field energy ($m_i v_{A,i}^2/2 \in [1, 10^4]$ eV), with ranges for environments presented in Table 1. This broad parametric range allows us to reveal several key trends, reinforcing widely discussed energy transformation mechanisms in current sheets (energy storage in the form of magnetic field, energy release in the form of plasma flows due to the reconnection, plasma flow thermalization, and kinetic energy transfer to thermal energy; see Y.-H. Liu et al., 2024; Pontin & Priest, 2022, and references therein):

- Investigated current sheets exhibit a general trend of kinetic energy increase with an increase of magnetic field (per particle) energy, and for protons at least for 80% of population $K_p \leq m_p v_{A,p}^2/2$. For heavy ion population in Martian magnetotail this was not the case: heavy ion flows result in $K_i > m_i v_{A,i}^2/2$.
- Majority of current sheets lay within $T_i \geq K_i$ and show a general trend of increase of T_i as K_i increases, with the exception of solar wind with median $T_i/K_i \approx 1$ and heavy ion population of Martian magnetotail with heavy ion flow $K_i > T_i$.
- Most current sheets are observed in the sub-sonic regime ($M < 1$), while Jovian and Martian magnetotails may contain super-sonic current sheets.

The distribution of current sheet in the $(\beta_{\max}, M_A)$ space is consistent with the existence of two primary equilibrium regimes (see also discussion in An et al., 2023; A. Artemyev et al., 2022):

Table 1
Estimated Ranges for Plasma Parameters Inside the Current Sheets

	$\beta_{\max}$	M_A	T_i/T_e	T_i, eV	K_i, eV	$m_i v_{A,i}^2/2$, eV
Earth magnetotail ($9R_E - 35R_E$)	10 – 500	0.07 – 1.4	2 – 8	$10^3 - 4 \cdot 10^3$	≤500	≤1500
Earth magnetotail ($65R_E - 170R_E$)	5 – 10^3	0.3 – 5	3 – 30	$200 - 3.3 \cdot 10^3$	≤1000	≤480
Earth's dayside magnetosheath	2 – 180	0.2 – 2	3 – 13	100 – 600	≤150	≤170
Earth's nightside magnetosheath	2 – 60	0.3 – 3	1.5 – 11	18 – 230	≤70	≤70
Solar wind (1 AU)	0.5 – 20	0.2 – 2	0.1 – 2.2	1.4 – 40	≤50	≤60
Martian magnetotail ($<3R_M$) H^+ ions	2 – 800	0.6 – 15	0.5 – 25	2.5 – 1000	≤300	≤1600
Martian magnetotail ($<3R_M$) O_2^+ ions	2 – 800	0.6 – 15	0.5 – 25	2.5 – 1450	≤2200	≤600
Jovian magnetotail ($30R_J - 105R_J$) H^+ ions	5 – 700	2 – 12	1 – 6	1600 – 7000	≤1800	$\leq 1.2 \cdot 10^4$

Note. Values estimated from distribution boundaries presented on Figures 2 and 3.

- Current sheets with high $\beta_{\max}$ $(\geq 10^2)$ are balanced predominantly by thermal pressure gradients ($4\pi\nabla P = [[\nabla \times \mathbf{B}] \times \mathbf{B}]$) and can be found in nearly stagnant plasma with $M_A \ll 1$. A typical example is the near-Earth magnetotail.
- Current sheets with moderate to small $\beta_{\max}$ (≤ 10) may have insufficient thermal pressure gradients to balance the magnetic tension force, requiring fast plasma flows for pressure balance ($4\pi m_i n(\mathbf{v}\cdot\nabla)\mathbf{v} = [[\nabla \times \mathbf{B}] \times \mathbf{B}]$) with $M_A \sim 1$. This scenario is characteristic of the solar wind and the Earth's distant magnetotail. Interestingly, current sheets in the Jovian and Martian magnetotails, typically embedded in fast flows ($M_A > 1$), can be balanced by plasma flows in the small $\beta_{\max}$ regime.

By combining T_i/T_e with $(\beta_{\max}, M_A)$ space, we can further classify current sheets. Except for the solar wind and certain portions of the Martian magnetotail, most current sheets are found in plasmas where ions are hotter than electrons ($T_i/T_e > 1$). The distinction ($T_i/T_e > 1$ vs. $T_i/T_e < 1$) becomes evident when examining the two-fluid equations for stationary current sheets.

For current sheets balanced by thermal pressure gradients, $4\pi\nabla P = [[\nabla \times \mathbf{B}] \times \mathbf{B}]$, ion and electron current densities follow:

$$\mathbf{j}_{i,e} = q_{i,e} nc \frac{\mathbf{E}\times\mathbf{B}}{B^2} + c\frac{\mathbf{B}\times\nabla P_{i,e}}{B^2},$$

where n is the plasma density and $q_{i,e} = \pm e$ are ion and electron charges. In intense (thin) current sheets, the main current carries are electrons (see theoretical explanations in Hesse et al. (1998), Zelenyi et al. (2010), and Lu et al. (2016), with observational confirmations in A. V. Artemyev et al. (2009) and Lu et al. (2019)). Under these conditions, the ion equation simplifies to $e\mathbf{E} = n^{-1}\nabla P_i$.

Current sheets with hot ions: In the limit of $T_i/T_e \gg 1$, the current density is primarily due to the Hall effect

$$\mathbf{j} \approx \mathbf{j}_e = -enc\frac{\mathbf{E}\times\mathbf{B}}{B^2}.$$

This scenario works in near-Earth magnetotail (e.g., Lu et al., 2019) and distant magnetotail (e.g., Kamaletdinov et al., 2024a), and is expected to apply to Martian and Jovian magnetotail current sheets with hot ions.

Current sheets with hot electrons: In the limit of $T_i/T_e \leq 1$ and for strongly anisotropic electrons, $T_{e\|}/T_{e\perp} \sim 1 + 2\beta_e^{-1}$, the current density is dominated by electron curvature drifts (A. V. Artemyev, Vasko, et al., 2016; Zelenyi et al., 2022)

$$\mathbf{j} \approx \mathbf{j}_e = \frac{1}{2}\beta_e\left(\frac{T_{e\|}}{T_{e\perp}} - 1\right)\frac{[\mathbf{B}\times(\mathbf{B}\cdot\nabla)\mathbf{B}]}{B^2}.$$

This mechanism works in the near-Earth (A. V. Artemyev, Angelopoulos, Liu, & Runov, 2017) and Jovian magnetotails (A. V. Artemyev et al., 2023), and is applicable to Martian magnetotail current sheets with hot electrons.

Low-β current sheets: For low-β thin current sheets the stress balance can be considered separately along $\mathbf{n}$ and $\mathbf{l}$ directions. Across current sheets (along $\mathbf{n}$) the stress balance is often provided by the force-free current sheet configuration with $\mathbf{j}\|\mathbf{B}$ within the current sheet plane (e.g., Neukirch, Vasko, et al., 2020; Vasko et al., 2022). Along $\mathbf{l}$ direction plasma flows dominate the stress balance, $4\pi m_i n(\mathbf{v}\cdot\nabla)\mathbf{v} = [[\nabla \times \mathbf{B}] \times \mathbf{B}]$. Such current sheets are mainly observed in the solar wind (where $T_i/T_e < 1$; see A. V. Artemyev, Angelopoulos, & Vasko, 2019; Vasko et al., 2022, for examples of current sheets with $\mathbf{j}\|\mathbf{B}$) and in the cold plasma of the Martian magnetotail (where T_i/T_e can reach one; see A. V. Artemyev, Angelopoulos, Halekas, et al., 2017, for examples of current sheets with $\mathbf{j}\|\mathbf{B}$).

Conclusions of our statistical study can be summarized as follows:

- Current sheet observations across Earth's space environment (solar wind, magnetosheath, and magnetotail) show a general trend of $T_i \gtrsim K_i$ and $m_i v_{A,i}^2/2 \sim K_i$. These correlations are less apparent for individual systems.

- The parameter space of current sheets in the Martian magnetotail well overlaps with that of Earth's space environment (about 40% of current sheets observed in Martian magnetotail appear within the $(M_A, \beta_{\max})$ parametric space determined by the Earth's magnetotail current sheets), making it an excellent testbed for current sheet investigations.
- Current sheets in the Jovian magnetotail occupy a parameter space (K_i, T_i, $m_i v_{A,i}^2/2$, d_i, and ρ_i) that is inaccessible in both Earth's space environment and Martian magnetotail. Low plasma density and hot heavy ion populations make the Jovian magnetotail a distinct environment for investigating current sheet structures and dynamics.

Data Availability Statement

THEMIS A-D FGM (Glassmeier et al., 2021), ESA (Carlson & McFadden, 2017b), MOM (Carlson & McFadden, 2017a) data sets, and MAVEN magnetic field data in Sun-State coordinates (Connerney, 2017) were accessed and processed using pySPEDAS V.1.7.3 (Grimes et al., 2024). MAVEN ion moments (STATIC, McFadden et al., 2015) and electron moments (SWEA, Mitchell et al., 2016) were accessed and processed using SPEDAS V4.1 (Angelopoulos et al., 2019, 2024). JUNO MAG (Connerney, 2024) and JADE-I L5 (R. J. Wilson, 2023) data was processed using pySPEDAS. Sunspot numbers data is available at Solar Influences Data analysis Center (SIDC) website (Clette & Lefèvre, 2015). Figures created using Matplotlib V.3.10.0 (Hunter, 2007; Team, 2024). Scikit-learn V.1.6.1 (Pedregosa et al., 2011) was used for One-Class SVM implementation. The complete set of events and processed data are archived at Zenodo repository (Tonoian, 2025).

Acknowledgments
We acknowledge the support of NASA contract NAS5-02099 for the use of data from the THEMIS Mission. Work of D.S.T., X.-J. Z., A.V.A., Q. M. are supported by NSF Grant 2400336 and NASA Grants 80NSSC23K0658, 80NSSC22K0752, 80NSSC22K1634. The work at Southwest Research Institute is funded by NASA's New Frontiers Program for Juno through contract NNM06AA75C.

References

An, X., Artemyev, A., Angelopoulos, V., Runov, A., & Kamaletdinov, S. (2023). Kinetic equilibrium of two-dimensional force-free current sheets. *The Astrophysical Journal*, *952*(1), 36. https://doi.org/10.3847/1538-4357/acdc1c

An, X., Artemyev, A., Angelopoulos, V., Runov, A., Lu, S., & Pritchett, P. (2022). Suppression of reconnection in polarized, thin magnetotail current sheets: 2D simulations and implications. *Physics of Plasmas*, *29*(9), 092901. https://doi.org/10.1063/5.0088064

Angelopoulos, V., Cruce, P., Drozdov, A., Grimes, E. W., Hatzigeorgiu, N., King, D. A., et al. (2019). The Space Physics Environment Data Analysis System (SPEDAS). *Space Science Reviews*, *215*(1), 9. https://doi.org/10.1007/s11214-018-0576-4

Angelopoulos, V., Cruce, P., Drozdov, A., Grimes, E. W., Hatzigeorgiu, N., King, D. A., et al. (2024). SPEDAS: Space Physics Environment Data Analysis System [Software]. *Astrophysics Source Code Library*. https://ui.adsabs.harvard.edu/abs/2024ascl.soft05001A/abstract

Angelopoulos, V., McFadden, J. P., Larson, D., Carlson, C. W., Mende, S. B., Frey, H., et al. (2008). Tail reconnection triggering substorm onset. *Science*, *321*(5891), 931–935. https://doi.org/10.1126/science.1160495

Angelopoulos, V., Sibeck, D., Carlson, C. W., McFadden, J. P., Larson, D., Lin, R. P., et al. (2008). First results from the THEMIS mission. *Space Science Reviews*, *141*(1–4), 453–476. https://doi.org/10.1007/s11214-008-9378-4

Arons, J. (2012). Pulsar wind nebulae as cosmic pevatrons: A current sheet's tale. *Space Science Reviews*, *173*(1–4), 341–367. https://doi.org/10.1007/s11214-012-9885-1

Artemyev, A., Reville, V., Zimovets, I., Nishimura, Y., Velli, M., Runov, A., & Angelopoulos, V. (2022). Thin current sheet formation: Comparison between Earth's magnetotail and coronal streamers. *arXiv e-prints*. arXiv:2205.01935. https://doi.org/10.48550/arXiv.2205.01935

Artemyev, A., Zimovets, I., Sharykin, I., Nishimura, Y., Downs, C., Weygand, J., et al. (2021). Comparative study of electric currents and energetic particle fluxes in a solar flare and Earth magnetospheric substorm. *The Astrophysical Journal*, *923*(2), 151. https://doi.org/10.3847/1538-4357/ac2dfc

Artemyev, A. V., Angelopoulos, V., Halekas, J. S., Runov, A., Zelenyi, L. M., & McFadden, J. P. (2017). Mars's magnetotail: Nature's current sheet laboratory. *Journal of Geophysical Research: Space Physics*, *122*(5), 5404–5417. https://doi.org/10.1002/2017JA024078

Artemyev, A. V., Angelopoulos, V., Hietala, H., Runov, A., & Shinohara, I. (2017). Ion density and temperature profiles along X_{GSM} and across Z_{GSM} the magnetotail as observed by THEMIS, Geotail, and ARTEMIS. *Journal of Geophysical Research*, *122*(2), 1590–1599. https://doi.org/10.1002/2016JA023710

Artemyev, A. V., Angelopoulos, V., Liu, J., & Runov, A. (2017). Electron currents supporting the near-Earth magnetotail during current sheet thinning. *Geophysical Research Letters*, *44*(1), 5–11. https://doi.org/10.1002/2016GL072011

Artemyev, A. V., Angelopoulos, V., & McTiernan, J. M. (2018). Near-Earth solar wind: Plasma characteristics from ARTEMIS measurements. *Journal of Geophysical Research: Space Physics*, *123*(12), 9955–9962. https://doi.org/10.1029/2018JA025904

Artemyev, A. V., Angelopoulos, V., & Runov, A. (2016). On the radial force balance in the quiet time magnetotail current sheet. *Journal of Geophysical Research: Space Physics*, *121*(5), 4017–4026. https://doi.org/10.1002/2016JA022480

Artemyev, A. V., Angelopoulos, V., Runov, A., & Vasko, I. Y. (2017). Hot ion flows in the distant magnetotail: ARTEMIS observations from lunar orbit to$\sim-$ 200 R_E. *Journal of Geophysical Research: Space Physics*, *122*(10), 9898–9909. https://doi.org/10.1002/2017JA024433

Artemyev, A. V., Angelopoulos, V., Runov, A., Wang, C.-P., & Zelenyi, L. M. (2017). Properties of the equatorial magnetotail flanks$\sim$ 50–200 R_E downtail. *Journal of Geophysical Research*, *122*(12), 11. https://doi.org/10.1002/2017JA024723

Artemyev, A. V., Angelopoulos, V., & Vasko, I. Y. (2019). Kinetic properties of solar wind discontinuities at 1 AU observed by ARTEMIS. *Journal of Geophysical Research: Space Physics*, *124*(6), 3858–3870. https://doi.org/10.1029/2019JA026597

Artemyev, A. V., Angelopoulos, V., Vasko, I.-Y., Runov, A., Avanov, L. A., Giles, B. L., et al. (2019). On the kinetic nature of solar wind discontinuities. *Geophysical Research Letters*, *46*(3), 1185–1194. https://doi.org/10.1029/2018GL079906

Artemyev, A. V., Baumjohann, W., Petrukovich, A. A., Nakamura, R., Dandouras, I., & Fazakerley, A. (2011). Proton/electron temperature ratio in the magnetotail. *Annales Geophysicae*, *29*(12), 2253–2257. https://doi.org/10.5194/angeo-29-2253-2011

Artemyev, A. V., Lu, S., El-Alaoui, M., Lin, Y., Angelopoulos, V., Zhang, X.-J., et al. (2021). Configuration of the Earth's magnetotail current sheet. *Geophysical Research Letters*, *48*(6), e92153. https://doi.org/10.1029/2020GL092153

Artemyev, A. V., Ma, Q., Ebert, R. W., Zhang, X. J., & Allegrini, F. (2023). Force-free current sheets in the Jovian magnetodisk: The key role of electron field-aligned anisotropy. *Journal of Geophysical Research: Space Physics*, *128*(3), e2022JA031280. https://doi.org/10.1029/2022JA031280

Artemyev, A. V., Petrukovich, A. A., Nakamura, R., & Zelenyi, L. M. (2011). Cluster statistics of thin current sheets in the Earth magnetotail: Specifics of the dawn flank, proton temperature profiles and electrostatic effects. *Journal of Geophysical Research*, *116*(A9), A0923. https://doi.org/10.1029/2011JA016801

Artemyev, A. V., Petrukovich, A. A., Nakamura, R., & Zelenyi, L. M. (2012). Adiabatic electron heating in the magnetotail current sheet: Cluster observations and analytical models. *Journal of Geophysical Research*, *117*(A6), A06219. https://doi.org/10.1029/2012JA017513

Artemyev, A. V., Petrukovich, A. A., Nakamura, R., & Zelenyi, L. M. (2015). Two-dimensional configuration of the magnetotail current sheet: THEMIS observations. *Geophysical Research Letters*, *42*(10), 3662–3667. https://doi.org/10.1002/2015GL063994

Artemyev, A. V., Petrukovich, A. A., Zelenyi, L. M., Nakamura, R., Malova, H. V., & Popov, V. Y. (2009). Thin embedded current sheets: Cluster observations of ion kinetic structure and analytical models. *Annales Geophysicae*, *27*(10), 4075–4087. https://doi.org/10.5194/angeo-27-4075-2009

Artemyev, A. V., Shi, C., Lin, Y., Nishimura, Y., Gonzalez, C., Verniero, J., et al. (2022). Ion kinetics of plasma flows: Earth's magnetosheath versus solar wind. *The Astrophysical Journal*, *939*(2), 85. https://doi.org/10.3847/1538-4357/ac96e4

Artemyev, A. V., Vasko, I. Y., Angelopoulos, V., & Runov, A. (2016). Effects of electron pressure anisotropy on current sheet configuration. *Physics of Plasmas*, *23*(9), 092901. https://doi.org/10.1063/1.4961926

Artemyev, A. V., Vasko, I. Y., & Kasahara, S. (2014). Thin current sheets in the Jovian magnetotail. *Planetary and Space Science*, *96*, 133–145. https://doi.org/10.1016/j.pss.2014.03.012

Aschwanden, M. J. (2002). Particle acceleration and kinematics in solar flares: A synthesis of recent observations and theoretical concepts. *Space Science Reviews*, *101*(1/2), 1–227. https://doi.org/10.1023/A:1019712124366

Auster, H. U., Glassmeier, K. H., Magnes, W., Aydogar, O., Baumjohann, W., Constantinescu, D., et al. (2008). The THEMIS fluxgate magnetometer. *Space Science Reviews*, *141*(1–4), 235–264. https://doi.org/10.1007/s11214-008-9365-9

Bagenal, F., Adriani, A., Allegrini, F., Bolton, S. J., Bonfond, B., Bunce, E. J., et al. (2017). Magnetospheric science objectives of the Juno mission. *Space Science Reviews*, *213*(1–4), 219–287. https://doi.org/10.1007/s11214-014-0036-8

Baker, D. N., Pulkkinen, T. I., Angelopoulos, V., Baumjohann, W., & McPherron, R. L. (1996). Neutral line model of substorms: Past results and present view. *Journal of Geophysical Research*, *101*(A6), 12975–13010. https://doi.org/10.1029/95JA03753

Barbhuiya, M. H., Cassak, P. A., Shay, M. A., Roytershteyn, V., Swisdak, M., Caspi, A., et al. (2022). Scaling of electron heating by magnetization during reconnection and applications to dipolarization fronts and super-hot solar flares. *Journal of Geophysical Research: Space Physics*, *127*(8), e30610. https://doi.org/10.1029/2022JA030610

Birn, J., & Hesse, M. (2005). Energy release and conversion by reconnection in the magnetotail. *Annales Geophysicae*, *23*(10), 3365–3373. https://doi.org/10.5194/angeo-23-3365-2005

Birn, J., & Hesse, M. (2014). Forced reconnection in the near magnetotail: Onset and energy conversion in PIC and MHD simulations. *Journal of Geophysical Research: Space Physics*, *119*(1), 290–309. https://doi.org/10.1002/2013JA019354

Carlson, C., & McFadden, J. (2017a). THEMIS Level 2 files for MOM (Moments for Electrostatic Analyzer) [Dataset]. *THEMIS*. Retrieved from https://themis.ssl.berkeley.edu/data/themis/

Carlson, C., & McFadden, J. (2017b). THEMIS Level 2 files for the ESA (Electrostatic Analyzer) instrument [Dataset]. *THEMIS*. Retrieved from https://themis.ssl.berkeley.edu/data/themis/

Carlsson, E., Fedorov, A., Barabash, S., Budnik, E., Grigoriev, A., Gunell, H., et al. (2006). Mass composition of the escaping plasma at Mars. *Icarus*, *182*(2), 320–328. https://doi.org/10.1016/j.icarus.2005.09.020

Cerutti, B., Werner, G. R., Uzdensky, D. A., & Begelman, M. C. (2014). Gamma-ray flares in the Crab Nebula: A case of relativistic reconnection? *Physics of Plasmas*, *21*(5), 056501. https://doi.org/10.1063/1.4872024

Chaston, C. C., Travnicek, P., & Russell, C. T. (2020). Turbulent wavefield morphology and ion scattering in the magnetosheath. *Geophysical Research Letters*, *47*(22), e89613. https://doi.org/10.1029/2020GL089613

Chen, C. H. K., & Boldyrev, S. (2017). Nature of kinetic scale turbulence in the Earth's magnetosheath. *The Astrophysical Journal*, *842*(2), 122. https://doi.org/10.3847/1538-4357/aa74e0

Chen, S.-H., Kivelson, M. G., Gosling, J. T., Walker, R. J., & Lazarus, A. J. (1993). Anomalous aspects of magnetosheath flow and of the shape and oscillations of the magnetopause during an interval of strongly northward interplanetary magnetic field. *Journal of Geophysical Research*, *98*(A4), 5727–5742. https://doi.org/10.1029/92JA02263

Clette, F., & Lefèvre, L. (2015). Silso sunspot number v2.0 [Dataset]. *WDC SILSO - Royal Observatory of Belgium (ROB)*. https://doi.org/10.24414/qnza-ac80

Connerney, J. (2017). MAVEN Tabulated vector magnetic field vs. time in Sun-state coordinates Data Collection [Dataset]. *NASA Planetary Data System*. https://doi.org/10.17189/1414251

Connerney, J. E. P. (2024). Juno MAG CALIBRATED DATA J V39 [Dataset]. *NASA Planetary Data System*. https://doi.org/10.17189/1414251

Connerney, J. E. P., Adriani, A., Allegrini, F., Bagenal, F., Bolton, S. J., Bonfond, B., et al. (2017). Jupiter's magnetosphere and aurorae observed by the Juno spacecraft during its first polar orbits. *Science*, *356*(6340), 826–832. https://doi.org/10.1126/science.aam5928

Connerney, J. E. P., Benn, M., Bjarno, J. B., Denver, T., Espley, J., Jorgensen, J. L., et al. (2017). The Juno magnetic field investigation. *Space Science Reviews*, *213*(1–4), 39–138. https://doi.org/10.1007/s11214-017-0334-z

Connerney, J. E. P., Espley, J., Lawton, P., Murphy, S., Odom, J., Oliversen, R., & Sheppard, D. (2015). The MAVEN magnetic field investigation. *Space Science Reviews*, *195*(1–4), 257–291. https://doi.org/10.1007/s11214-015-0169-4

Connerney, J. E. P., Espley, J. R., DiBraccio, G. A., Gruesbeck, J. R., Oliversen, R. J., Mitchell, D. L., et al. (2015). First results of the MAVEN magnetic field investigation. *Geophysical Research Letters*, *42*(21), 8819–8827. https://doi.org/10.1002/2015GL065366

Curry, S. M., Tatum, P., Mitchell, D., Luhmann, J. G., McFadden, J., Ruhunusiri, S., et al. (2022). Ion acceleration in Mars' twisted magnetotail. *Monthly Notices of the Royal Astronomical Society*, *517*(1), L121–L125. https://doi.org/10.1093/mnrasl/slac099

De Keyser, J., & Roth, M. (1998). Equilibrium conditions and magnetic field rotation at the tangential discontinuity magnetopause. *Journal of Geophysical Research*, *103*(A4), 6653–6662. https://doi.org/10.1029/97JA03710

DiBraccio, G. A., Espley, J. R., Gruesbeck, J. R., Connerney, J. E. P., Brain, D. A., Halekas, J. S., et al. (2015). Magnetotail dynamics at Mars: Initial MAVEN observations. *Geophysical Research Letters*, *42*(21), 8828–8837. https://doi.org/10.1002/2015GL065248

Dubinin, E., & Fraenz, M. (2015). Magnetotails of Mars and Venus. In A. Keiling, C. M. Jackman, & P. A. Delamere (Eds.), *Magnetotails in the solar system* (Vol. 207, pp. 34–59). https://doi.org/10.1002/9781118842324.ch3

Dubinin, E., Fraenz, M., Fedorov, A., Lundin, R., Edberg, N., Duru, F., & Vaisberg, O. (2011). Ion energization and escape on Mars and Venus. *Space Science Reviews*, *162*(1–4), 173–211. https://doi.org/10.1007/s11214-011-9831-7

Dubinin, E., Fraenz, M., Zhang, T. L., Woch, J., Wei, Y., Fedorov, A., et al. (2013). Plasma in the near Venus tail: Venus Express observations. *Journal of Geophysical Research: Space Physics*, *118*(12), 7624–7634. https://doi.org/10.1002/2013JA019164

Eastwood, J. P., Phan, T. D., Drake, J. F., Shay, M. A., Borg, A. L., Lavraud, B., & Taylor, M. G. G. T. (2013). Energy partition in magnetic reconnection in Earth's magnetotail. *Physical Review Letters*, *110*(22), 225001. https://doi.org/10.1103/PhysRevLett.110.225001

Erkaev, N. V., Farrugia, C. J., Harris, B., & Biernat, H. K. (2011). On accelerated magnetosheath flows under northward IMF. *Geophysical Research Letters*, *38*(1), L01104. https://doi.org/10.1029/2010GL045998

Fedorov, A., Budnik, E., Sauvaud, J.-A., Mazelle, C., Barabash, S., Lundin, R., et al. (2006). Structure of the martian wake. *Icarus*, *182*(2), 329–336. https://doi.org/10.1016/j.icarus.2005.09.021

Forbes, T. G. (2001). The nature of Petschek-type reconnection. *Earth, Planets and Space*, *53*(6), 423–429. https://doi.org/10.1186/BF03353252

Gershman, D. J., Fuselier, S. A., Cohen, I. J., Turner, D. L., Liu, Y.-H., Chen, L.-J., et al. (2024). Magnetic reconnection at planetary bodies and astrospheres. *Space Science Reviews*, *220*(1), 7. https://doi.org/10.1007/s11214-023-01017-2

Glassmeier, K. H., Auster, U., & Baumjohann, W. (2021). THEMIS level 2 files for the FGM (fluxgate magnetometer) instrument [Dataset]. *Themis*. Retrieved from https://themis.ssl.berkeley.edu/data/themis/

Goertz, C., & Baumjohann, W. (1991). On the thermodynamics of the plasma sheet. *Journal of Geophysical Research*, *96*(A12), 20991–20998. https://doi.org/10.1029/91ja02128

Gonzalez, W., & Parker, E. (2016). Magnetic reconnection (Vol. *427*). https://doi.org/10.1007/978-3-319-26432-5

Gosling, J. T. (2012). Magnetic reconnection in the solar wind. *Space Science Reviews*, *172*(1–4), 187–200. https://doi.org/10.1007/s11214-011-9747-2

Grigorenko, E. E., Zelenyi, L. M., DiBraccio, G., Ermakov, V. N., Shuvalov, S. D., Malova, H. V., et al. (2019). Thin current sheets of sub-ion scales observed by MAVEN in the Martian magnetotail. *Geophysical Research Letters*, *46*(12), 6214–6222. https://doi.org/10.1029/2019GL082709

Grigorenko, E. E., Zelenyi, L. M., Shuvalov, S. D., Malova, H. V., & Dubinin, E. (2022). Electron-scale current layers in the Martian magnetotail: Spatial scaling and properties of embedding. *The Astrophysical Journal*, *926*(2), 160. https://doi.org/10.3847/1538-4357/ac4bd8

Grimes, E. W., Hatzigeorgiu, N., Lewis, J. W., Russell, C., McTiernan, J. M., Drozdov, A., & Angelopoulos, V. (2024). pySPEDAS: Python-based Space Physics Environment Data Analysis Software [Software]. *Astrophysics Source Code Library*. https://ui.adsabs.harvard.edu/abs/2024ascl.soft05005G/abstract

Guo, F., Liu, Y.-H., Zenitani, S., & Hoshino, M. (2024). Magnetic reconnection and associated particle acceleration in high-energy astrophysics. *Space Science Reviews*, *220*(4), 43. https://doi.org/10.1007/s11214-024-01073-2

Harada, Y., Halekas, J. S., McFadden, J. P., Mitchell, D. L., Mazelle, C., Connerney, J. E. P., et al. (2015). Marsward and tailward ions in the near-Mars magnetotail: MAVEN observations. *Geophysical Research Letters*, *42*(21), 8925–8932. https://doi.org/10.1002/2015GL065005

Harada, Y., Halekas, J. S., Xu, S., DiBraccio, G. A., Ruhunusiri, S., Hara, T., et al. (2020). Ion jets within current sheets in the Martian magnetosphere. *Journal of Geophysical Research: Space Physics*, *125*(12), e28576. https://doi.org/10.1029/2020JA028576

Harris, B., Farrugia, C. J., Erkaev, N. V., & Torbert, R. B. (2013). Observational aspects of IMF draping-related magnetosheath accelerations for northward IMF. *Annales Geophysicae*, *31*(10), 1779–1789. https://doi.org/10.5194/angeo-31-1779-2013

Hasegawa, H. (2012). Structure and dynamics of the magnetopause and its boundary layers. *Monographs on Environment, Earth and Planets*, *1*(2), 71–119. https://doi.org/10.5047/meep.2012.00102.0071

Hesse, M., Winske, D., & Birn, J. (1998). On the ion-scale structure of thin current sheets in the magnetotail. *Physica Scripta*, *T74*, 63–66. https://doi.org/10.1088/0031-8949/1998/T74/012

Hietala, H., Drake, J. F., Phan, T. D., Eastwood, J. P., & McFadden, J. P. (2015). Ion temperature anisotropy across a magnetotail reconnection jet. *Geophysical Research Letters*, *42*(18), 7239–7247. https://doi.org/10.1002/2015GL065168

Hoshino, M., & Higashimori, K. (2015). Generation of Alfvénic waves and turbulence in reconnection jets. *Journal of Geophysical Research: Space Physics*, *120*(5), 3715–3727. https://doi.org/10.1002/2014JA020520

Hoshino, M., & Lyubarsky, Y. (2012). Relativistic reconnection and particle acceleration. *Space Science Reviews*, *173*(1–4), 521–533. https://doi.org/10.1007/s11214-012-9931-z

Hoshino, M., Mukai, T., Shinohara, I., Saito, Y., & Kokubun, S. (2000). Slow shock downstream structure in the magnetotail. *Journal of Geophysical Research*, *105*(A1), 337–348. https://doi.org/10.1029/1999JA900426

Hoshino, M., Nishida, A., Mukai, T., Saito, Y., Yamamoto, T., & Kokubun, S. (1996). Structure of plasma sheet in magnetotail: Double-peaked electric current sheet. *Journal of Geophysical Research*, *101*(A11), 24775–24786. https://doi.org/10.1029/96JA02313

Hunter, J. D. (2007). Matplotlib: A 2D graphics environment. *Computing in Science & Engineering*, *9*(3), 90–95. https://doi.org/10.1109/MCSE.2007.55

Huscher, E., Bagenal, F., Wilson, R. J., Allegrini, F., Ebert, R. W., Valek, P. W., et al. (2021). Survey of Juno observations in Jupiter's plasma disk: Density. *Journal of Geophysical Research: Space Physics*, *126*(8), e29446. https://doi.org/10.1029/2021JA029446

Inui, S., Seki, K., Namekawa, T., Sakai, S., Brain, D. A., Hara, T., et al. (2018). Cold dense ion outflow observed in the Martian-induced magnetotail by MAVEN. *Geophysical Research Letters*, *45*(11), 5283–5289. https://doi.org/10.1029/2018GL077584

Jackman, C. M., Arridge, C. S., André, N., Bagenal, F., Birn, J., Freeman, M. P., et al. (2014). Large-scale structure and dynamics of the magnetotails of Mercury, Earth, Jupiter and Saturn. *Space Science Reviews*, *182*, 85–154. https://doi.org/10.1007/s11214-014-0060-8

Juusola, L., Østgaard, N., & Tanskanen, E. (2011). Statistics of plasma sheet convection. *Journal of Geophysical Research*, *116*(A8), A08201. https://doi.org/10.1029/2011JA016479

Juusola, L., Østgaard, N., Tanskanen, E., Partamies, N., & Snekvik, K. (2011). Earthward plasma sheet flows during substorm phases. *Journal of Geophysical Research*, *116*(A10), A10228. https://doi.org/10.1029/2011JA016852

Kamaletdinov, S. R., Artemyev, A. V., Runov, A., & Angelopoulos, V. (2024a). Characteristics of thin magnetotail current sheet plasmas at lunar distances. *Journal of Geophysical Research: Space Physics*, *129*(8), e2024JA032755. https://doi.org/10.1029/2024JA032755

Kamaletdinov, S. R., Artemyev, A. V., Runov, A., & Angelopoulos, V. (2024b). Thin current sheets in the magnetotail at lunar distances: Statistics of ARTEMIS observations. *Journal of Geophysical Research: Space Physics*, *129*(3), e2023JA032130. https://doi.org/10.1029/2023JA032130

Karimabadi, H., Roytershteyn, V., Mouikis, C. G., Kistler, L. M., & Daughton, W. (2011). Flushing effect in reconnection: Effects of minority species of oxygen ions. *Planetary and Space Science*, *59*(7), 526–536. https://doi.org/10.1016/j.pss.2010.07.014

Kasahara, S., Kronberg, E. A., Kimura, T., Tao, C., Badman, S. V., Masters, A., et al. (2013). Asymmetric distribution of reconnection jet fronts in the Jovian nightside magnetosphere. *Journal of Geophysical Research: Space Physics*, *118*(1), 375–384. https://doi.org/10.1029/2012JA018130

Kasahara, S., Kronberg, E. A., Krupp, N., Kimura, T., Tao, C., Badman, S. V., et al. (2011). Magnetic reconnection in the Jovian tail: X-line evolution and consequent plasma sheet structures. *Journal of Geophysical Research*, *116*(A11), 11219. https://doi.org/10.1029/2011JA016892

Khabarova, O., Malandraki, O., Malova, H., Kislov, R., Greco, A., Bruno, R., et al. (2021). Current sheets, plasmoids and flux ropes in the heliosphere. Part I. 2-D or not 2-D? General and observational aspects. *Space Science Reviews*, *217*(3), 38. https://doi.org/10.1007/s11214-021-00814-x

Kim, T. K., Ebert, R. W., Valek, P. W., Allegrini, F., McComas, D. J., Bagenal, F., et al. (2020a). Method to derive ion properties from Juno JADE including abundance estimates for O^+ and S^{2+}. *Journal of Geophysical Research: Space Physics*, *125*(2), e26169. https://doi.org/10.1029/2018JA026169

Kim, T. K., Ebert, R. W., Valek, P. W., Allegrini, F., McComas, D. J., Bagenal, F., et al. (2020b). Survey of ion properties in Jupiter's plasma sheet: Juno JADE-I observations. *Journal of Geophysical Research: Space Physics*, *125*(4), e27696. https://doi.org/10.1029/2019JA027696

King, J. H., & Papitashvili, N. E. (2005). Solar wind spatial scales in and comparisons of hourly Wind and ACE plasma and magnetic field data. *Journal of Geophysical Research*, *110*(A2), A02104. https://doi.org/10.1029/2004JA010649

Kissinger, J., McPherron, R. L., Hsu, T.-S., & Angelopoulos, V. (2012). Diversion of plasma due to high pressure in the inner magnetosphere during steady magnetospheric convection. *Journal of Geophysical Research*, *117*(A5), 5206. https://doi.org/10.1029/2012JA017579

Kistler, L. M., Mouikis, C., MöBius, E., Klecker, B., Sauvaud, J. A., RéMe, H., et al. (2005). Contribution of nonadiabatic ions to the cross-tail current in an O^+ dominated thin current sheet. *Journal of Geophysical Research*, *110*(A6), 6213. https://doi.org/10.1029/2004JA010653

Kropotina, J. A., Webster, L., Artemyev, A. V., Bykov, A. M., Vainchtein, D. L., & Vasko, I. Y. (2021). Solar wind discontinuity transformation at the bow shock. *The Astrophysical Journal*, *913*(2), 142. https://doi.org/10.3847/1538-4357/abf6c7

Krupp, N., Kronberg, E., & Radioti, A. (2015). Jupiter's magnetotail. In *Magnetotails in the solar system* (pp. 85–98). American Geophysical Union (AGU). https://doi.org/10.1002/9781118842324.ch5

Kulsrud, R. M. (2001). Magnetic reconnection: Sweet-Parker versus Petschek. *Earth, Planets and Space*, *53*(6), 417–422. https://doi.org/10.1186/BF03353251

Li, X. Z., Rong, Z. J., Fraenz, M., Zhang, C., Klinger, L., Shi, Z., et al. (2023). Two types of Martian magnetotail current sheets: MAVEN observations of ion composition. *Geophysical Research Letters*, *50*(2), e2022GL102630. https://doi.org/10.1029/2022GL102630

Liang, H., Ashour-Abdalla, M., Lapenta, G., & Walker, R. J. (2016). Oxygen impacts on dipolarization fronts and reconnection rate. *Journal of Geophysical Research: Space Physics*, *121*, 1148–1166. https://doi.org/10.1002/2015JA021747

Liu, Y.-H., Hesse, M., Genestreti, K., Nakamura, R., Burch, J., Cassak, P., et al. (2024). Ohm's law, the reconnection rate, and energy conversion in collisionless magnetic reconnection. *arXiv e-prints*. arXiv:2406.00875. https://doi.org/10.48550/arXiv.2406.00875

Liu, Y. Y., Fu, H. S., Cao, J. B., Wang, Z., He, R. J., Guo, Z. Z., et al. (2022). Magnetic discontinuities in the solar wind and magnetosheath: Magnetospheric multiscale mission (MMS) observations. *The Astrophysical Journal*, *930*(1), 63. https://doi.org/10.3847/1538-4357/ac62d2

Liu, Z. Y., Blanc, M., Andre, N., Bagenal, F., Wilson, R. J., Allegrini, F., et al. (2024). Juno observations of Jupiter's magnetodisk plasma: Implications for equilibrium and dynamics. *Journal of Geophysical Research: Space Physics*, *129*(11), 2024JA032976. https://doi.org/10.1029/2024JA032976

Liu, Z. Y., Zong, Q. G., Blanc, M., Sun, Y. X., Zhao, J. T., Hao, Y. X., & Mauk, B. H. (2021). Statistics on Jupiter's current sheet with Juno data: Geometry, magnetic fields and energetic particles. *Journal of Geophysical Research: Space Physics*, *126*(11), e29710. https://doi.org/10.1029/2021JA029710

Lu, S., Pritchett, P. L., Angelopoulos, V., & Artemyev, A. V. (2018). Magnetic reconnection in Earth's magnetotail: Energy conversion and its earthward-tailward asymmetry. *Physics of Plasmas*, *25*(1), 012905. https://doi.org/10.1063/1.5016435

Lu, S., Angelopoulos, V., Artemyev, A. V., Jia, Y., Chen, Q., Liu, J., & Runov, A. (2020). Magnetic reconnection in a charged, electron-dominant current sheet. *Physics of Plasmas*, *27*(10), 102902. https://doi.org/10.1063/5.0020857

Lu, S., Artemyev, A. V., Angelopoulos, V., Lin, Y., Zhang, X. J., Liu, J., et al. (2019). The Hall electric field in Earth's magnetotail thin current sheet. *Journal of Geophysical Research: Space Physics*, *124*(2), 1052–1062. https://doi.org/10.1029/2018JA026202

Lu, S., Lin, Y., Angelopoulos, V., Artemyev, A. V., Pritchett, P. L., Lu, Q., & Wang, X. Y. (2016). Hall effect control of magnetotail dawn-dusk asymmetry: A three-dimensional global hybrid simulation. *Journal of Geophysical Research: Space Physics*, *121*(12), 11882–11895. https://doi.org/10.1002/2016JA023325

Lui, A. T. Y. (2004). Potential plasma instabilities for substorm expansion onsets. *Space Science Reviews*, *113*(1/2), 127–206. https://doi.org/10.1023/B:SPAC.0000042942.00362.4e

Lukin, A., Guo, Z., Lin, Y., Panov, E., Artemyev, A., Zhang, X., & Petrukovich, A. (2024). Triggering the magnetopause reconnection by solar wind discontinuities. *The Astrophysical Journal*, *963*(2), 145. https://doi.org/10.3847/1538-4357/ad1e63

Lukin, A. S., Panov, E. V., Artemyev, A. V., Petrukovich, A. A., Haaland, S., Nakamura, R., et al. (2020). Comparison of the flank magnetopause at near-Earth and lunar distances: MMS and ARTEMIS observations. *Journal of Geophysical Research: Space Physics*, *125*(11), e28406. https://doi.org/10.1029/2020JA028406

Maes, L., Fraenz, M., McFadden, J. P., & Benna, M. (2021). Escape of CO_2^+ and other heavy minor ions from the ionosphere of Mars. *Journal of Geophysical Research: Space Physics*, *126*(1), e28608. https://doi.org/10.1029/2020JA028608

McComas, D. J., Alexander, N., Allegrini, F., Bagenal, F., Beebe, C., Clark, G., et al. (2017). The Jovian auroral distributions experiment (JADE) on the Juno mission to Jupiter. *Space Science Reviews*, *213*(1–4), 547–643. https://doi.org/10.1007/s11214-013-9990-9

McComas, D. J., Szalay, J. R., Allegrini, F., Bagenal, F., Connerney, J., Ebert, R. W., et al. (2017). Plasma environment at the dawn flank of Jupiter's magnetosphere: Juno arrives at Jupiter. *Geophysical Research Letters*, *44*(10), 4432–4438. https://doi.org/10.1002/2017GL072831

McFadden, J. P., Carlson, C. W., Larson, D., Ludlam, M., Abiad, R., Elliott, B., et al. (2008). The THEMIS ESA plasma instrument and in-flight calibration. *Space Science Reviews*, *141*(1–4), 277–302. https://doi.org/10.1007/s11214-008-9440-2

McFadden, J. P., Kortmann, O., Curtis, D., Dalton, G., Johnson, G., Abiad, R., et al. (2015). MAVEN suprathermal and thermal ion compostion (STATIC) instrument. *Space Science Reviews*, *195*(1–4), 199–256. https://doi.org/10.1007/s11214-015-0175-6

Mitchell, D. L., Mazelle, C., Sauvaud, J.-A., Thocaven, J.-J., Rouzaud, J., Fedorov, A., et al. (2016). The MAVEN solar wind electron analyzer. *Space Science Reviews*, *200*(1–4), 495–528. https://doi.org/10.1007/s11214-015-0232-1

Mouikis, C. G., Kistler, L. M., Liu, Y. H., Klecker, B., Korth, A., & Dandouras, I. (2010). $H^+$and O^+ content of the plasma sheet at 15–19 Re as a function of geomagnetic and solar activity. *Journal of Geophysical Research*, *115*(A12), A00J16. https://doi.org/10.1029/2010JA015978

Nakamura, R., Burch, J. L., Birn, J., Chen, L. J., Graham, D. B., Guo, F., et al. (2024). Outstanding questions and future research of magnetic reconnection. *arXiv e-prints*. arXiv:2407.09670. https://doi.org/10.48550/arXiv.2407.09670

Neukirch, T., Vasko, I. Y., Artemyev, A. V., & Allanson, O. (2020). Kinetic models of tangential discontinuities in the solar wind. *The Astrophysical Journal*, *891*(1), 86. https://doi.org/10.3847/1538-4357/ab7234

Neukirch, T., Wilson, F., & Allanson, O. (2020). A family of Vlasov-Maxwell equilibrium distribution functions describing a transition from the Harris sheet to the force-free Harris sheet. *Journal of Plasma Physics*, *86*(3), 825860302. https://doi.org/10.1017/S0022377820000604

Øieroset, M., Phan, T. D., Drake, J. F., Starkey, M., Fuselier, S. A., Cohen, I. J., et al. (2024). Scaling of ion bulk heating in magnetic reconnection outflows for the high-Alfvén-speed and low-β regime in Earth's magnetotail. *The Astrophysical Journal*, *971*(2), 144. https://doi.org/10.3847/1538-4357/ad6151

Oka, M., Birn, J., Egedal, J., Guo, F., Ergun, R. E., Turner, D. L., et al. (2023). Particle acceleration by magnetic reconnection in geospace. *Space Science Reviews*, *219*(8), 75. https://doi.org/10.1007/s11214-023-01011-8

Panov, E. V., Artemyev, A. V., Nakamura, R., & Baumjohann, W. (2011). Two types of tangential magnetopause current sheets: Cluster observations and theory. *Journal of Geophysical Research*, *116*(A12), A12204. https://doi.org/10.1029/2011JA016860

Parker, E. N. (1994). *Spontaneous current sheets in magnetic fields: With applications to stellar x-rays. Spontaneous current sheets in magnetic fields: With applications to stellar X-rays. International Series in Astronomy and Astrophysics* (Vol. 1, p. 1). Oxford University Press.

Pedregosa, F., Varoquaux, G., Gramfort, A., Michel, V., Thirion, B., Grisel, O., et al. (2011). Scikit-learn: Machine learning in Python. *Journal of Machine Learning Research*, *12*, 2825–2830.

Petrukovich, A. A., Artemyev, A. V., Vasko, I. Y., Nakamura, R., & Zelenyi, L. M. (2015). Current sheets in the Earth magnetotail: Plasma and magnetic field structure with Cluster project observations. *Space Science Reviews*, *188*(1–4), 311–337. https://doi.org/10.1007/s11214-014-0126-7

Petrukovich, A. A., Mukai, T., Kokubun, S., Romanov, S. A., Saito, Y., Yamamoto, T., & Zelenyi, L. M. (1999). Substorm-associated pressure variations in the magnetotail plasma sheet and lobe. *Journal of Geophysical Research*, *104*, 4501–4514. https://doi.org/10.1029/98JA02418

Pezzi, O., Pecora, F., Le Roux, J., Engelbrecht, N. E., Greco, A., Servidio, S., et al. (2021). Current sheets, plasmoids and flux ropes in the heliosphere. Part II: Theoretical aspects. *Space Science Reviews*, *217*(3), 39. https://doi.org/10.1007/s11214-021-00799-7

Phan, T. D., Bale, S. D., Eastwood, J. P., Lavraud, B., Drake, J. F., Oieroset, M., et al. (2020). Parker solar probe in situ observations of magnetic reconnection exhausts during encounter 1. *The Astrophysical Journal Supplement Series*, *246*(2), 34. https://doi.org/10.3847/1538-4365/ab55ee

Phan, T. D., Drake, J. F., Shay, M. A., Gosling, J. T., Paschmann, G., Eastwood, J. P., et al. (2014). Ion bulk heating in magnetic reconnection exhausts at Earth's magnetopause: Dependence on the inflow Alfvén speed and magnetic shear angle. *Geophysical Research Letters*, *41*(20), 7002–7010. https://doi.org/10.1002/2014GL061547

Phan, T. D., Eastwood, J. P., Shay, M. A., Drake, J. F., Sonnerup, B. U. Ö., Fujimoto, M., et al. (2018). Electron magnetic reconnection without ion coupling in Earth's turbulent magnetosheath. *Nature*, *557*(7704), 202–206. https://doi.org/10.1038/s41586-018-0091-5

Phan, T. D., Gosling, J. T., Davis, M. S., Skoug, R. M., Øieroset, M., Lin, R. P., et al. (2006). A magnetic reconnection X-line extending more than 390 Earth radii in the solar wind. *Nature*, *439*(7073), 175–178. https://doi.org/10.1038/nature04393

Pontin, D. I., & Priest, E. R. (2022). Magnetic reconnection: MHD theory and modelling. *Living Reviews in Solar Physics*, *19*(1), 1. https://doi.org/10.1007/s41116-022-00032-9

Priest, E. R. (1985). The magnetohydrodynamics of current sheets. *Reports on Progress in Physics*, *48*(7), 955–1090. https://doi.org/10.1088/0034-4885/48/7/002

Pritchett, P. L., & Coroniti, F. V. (2011). Plasma sheet disruption by interchange-generated flow intrusions. *Geophysical Research Letters*, *38*(10), 10102. https://doi.org/10.1029/2011GL047527

Quartey, N. A., & Liemohn, M. W. (2025). Multispecies MHD simulations of the crustal field influence at the Mars magnetotail current sheet. *Journal of Geophysical Research: Space Physics*, *130*(4), e2024JA033445. https://doi.org/10.1029/2024JA033445

Runov, A., Angelopoulos, V., Artemyev, A. V., Weygand, J. M., Lu, S., Lin, Y., & Zhang, X. J. (2021). Global and local processes of thin current sheet formation during substorm growth phase. *Journal of Atmospheric and Solar-Terrestrial Physics*, *220*, 105671. https://doi.org/10.1016/j.jastp.2021.105671

Runov, A., Sergeev, V. A., Nakamura, R., Baumjohann, W., Apatenkov, S., Asano, Y., et al. (2006). Local structure of the magnetotail current sheet: 2001 cluster observations. *Annales Geophysicae*, *24*(1), 247–262. https://doi.org/10.5194/angeo-24-247-2006

Sahraoui, F., Belmont, G., Rezeau, L., Cornilleau-Wehrlin, N., Pinçon, J. L., & Balogh, A. (2006). Anisotropic turbulent spectra in the terrestrial magnetosheath as seen by the cluster spacecraft. *Physical Review Letters*, *96*(7), 075002. https://doi.org/10.1103/PhysRevLett.96.075002

Schölkopf, B., Platt, J. C., Shawe-Taylor, J., Smola, A. J., & Williamson, R. C. (2001). Estimating the support of a high-dimensional distribution. *Neural Computation*, *13*(7), 1443–1471. https://doi.org/10.1162/089976601750264965

Sergeev, V. A., Angelopoulos, V., Carlson, C., & Sutcliffe, P. (1998). Current sheet measurements within a flapping plasma sheet. *Journal of Geophysical Research*, *103*(A5), 9177–9188. https://doi.org/10.1029/97JA02093

Shen, Y., Artemyev, A., Angelopoulos, V., Liu, T. Z., & Vasko, I. (2024). Comparing plasma anisotropy associated with solar wind discontinuities and Alfvénic fluctuations. *The Astrophysical Journal*, *961*(1), 41. https://doi.org/10.3847/1538-4357/ad110b

Shi, C. (2022). Instabilities in a current sheet with plasma jet. *Journal of Plasma Physics*, *88*(4), 555880401. https://doi.org/10.1017/S0022377822000575

Shi, C., Artemyev, A., Velli, M., & Tenerani, A. (2021). Stability of the magnetotail current sheet with normal magnetic field and field-aligned plasma flows. *Journal of Geophysical Research: Space Physics*, *126*(11), e29711. https://doi.org/10.1029/2021JA029711

Shustov, P. I., Lukin, A. S., Zhang, X. J., Artemyev, A. V., Petrukovich, A. A., & Angelopoulos, V. (2021). Evolution of thermal electron distributions in the magnetotail: Convective heating and scattering-induced losses. *Journal of Geophysical Research: Space Physics*, *126*(12), e29952. https://doi.org/10.1029/2021JA029952

Sitnov, M. I., & Arnold, H. (2025). Reconnection onset in overstretched thin current sheets: Pic simulations. *Journal of Geophysical Research: Space Physics*, *130*(5), e2025JA033863. https://doi.org/10.1029/2025JA033863

Sitnov, M. I., Birn, J., Ferdousi, B., Gordeev, E., Khotyaintsev, Y., Merkin, V., et al. (2019). Explosive magnetotail activity. *Space Science Reviews*, *215*(4), 31. https://doi.org/10.1007/s11214-019-0599-5

Sitnov, M. I., & Merkin, V. G. (2016). Generalized magnetotail equilibria: Effects of the dipole field, thin current sheets, and magnetic flux accumulation. *Journal of Geophysical Research*, *121*(8), 7664–7683. https://doi.org/10.1002/2016JA023001

Sonnerup, B. U. Ö., & Scheible, M. (2000). In G. Paschmann & W. D. Patrick (Eds.), *ISSI book on analysis methods for multi-spacecraft data* (Vol. 449).

Syrovatskii, S. I. (1981). Pinch sheets and reconnection in astrophysics. *Annual Review of Astronomy and Astrophysics*, *19*(1), 163–229. https://doi.org/10.1146/annurev.aa.19.090181.001115

Team, T. M. D. (2024). Matplotlib: Visualization with Python [Software]. *Zenodo*. https://doi.org/10.5281/zenodo.14464227

Tonoian, D. (2025). Datasets of current sheet crossings for comparative analysis of current sheets in Earth magnetosphere, Martian and Jovian magnetotails [Dataset]. *Zenodo*. https://doi.org/10.5281/zenodo.14984931

Vasko, I. Y., Alimov, K., Phan, T., Bale, S. D., Mozer, F. S., & Artemyev, A. V. (2022). Kinetic-scale current sheets in the solar wind at 1 au: Scale-dependent properties and critical current density. *The Astrophysical Journal Letters*, *926*(2), L19. https://doi.org/10.3847/2041-8213/ac4fc4

Vasko, I. Y., Petrukovich, A. A., Artemyev, A. V., Nakamura, R., & Zelenyi, L. M. (2015). Earth's distant magnetotail current sheet near and beyond lunar orbit. *Journal of Geophysical Research: Space Physics*, *120*(10), 8663–8680. https://doi.org/10.1002/2015JA021633

Vasquez, B. J., Abramenko, V. I., Haggerty, D. K., & Smith, C. W. (2007). Numerous small magnetic field discontinuities of Bartels rotation 2286 and the potential role of Alfvénic turbulence. *Journal of Geophysical Research*, *112*(A11), A11102. https://doi.org/10.1029/2007JA012504

Vasquez, B. J., & Hollweg, J. V. (2001). Evolution and dissipation of imbedded rotational discontinuities and Alfvén waves in nonuniform plasma and the resultant proton heating. *Journal of Geophysical Research*, *106*, 5661–5682. https://doi.org/10.1029/2000JA000268

Walia, N. K., Seki, K., Amano, T., Kitamura, N., Saito, Y., Ahmadi, T., et al. (2024). A study of slow-mode shocks in the near-Earth magnetotail with MMS observations and hybrid simulations. *The Astrophysical Journal*, *977*(1), 117. https://doi.org/10.3847/1538-4357/ad8b23

Wang, C.-P., Gkioulidou, M., Lyons, L. R., & Angelopoulos, V. (2012). Spatial distributions of the ion to electron temperature ratio in the magnetosheath and plasma sheet. *Journal of Geophysical Research*, *117*(A8), 8215. https://doi.org/10.1029/2012JA017658

Wang, J.-Z., Bagenal, F., Wilson, R. J., Nerney, E., Crary, F., Dols, V., et al. (2024). Forward modeling of 3-D ion properties in Jupiter's magnetosphere using Juno/JADE-I data. *Journal of Geophysical Research: Space Physics*, *129*(4), e2023JA032218. https://doi.org/10.1029/2023JA032218

Wang, J.-Z., Bagenal, F., Wilson, R. J., Valek, P. W., Ebert, R. W., & Allegrini, F. (2024). Ion parameters dataset from Juno/JADE observations in Jupiter's magnetosphere between 10 and 50 R_J. *Journal of Geophysical Research: Space Physics*, *129*(12), 2024JA033454. https://doi.org/10.1029/2024JA033454

Wang, R., Vasko, I. Y., Phan, T., & Mozer, F. S. (2024). Solar wind current sheets: Mva inaccuracy and recommended single-spacecraft methodology. *Journal of Geophysical Research: Space Physics*, *129*(2), e2023JA032215. https://doi.org/10.1029/2023ja032215

Wilson, L. B., III, Stevens, M. L., Kasper, J. C., Klein, K. G., Maruca, B. A., Bale, S. D., et al. (2018). The statistical properties of solar wind temperature parameters near 1 au. *The Astrophysical Journal Supplement Series*, *236*, 41. https://doi.org/10.3847/1538-4365/aab71c

Wilson, R. J. (2023). Juno J/sw Jovian Auroral Distribution Def V1.0 [Dataset]. *NASA Planetary Data System, JNO-J/SW-JAD-5-CALIBRATED-V1.0*. https://doi.org/10.17189/2775-4623

Xu, S., Runov, A., Artemyev, A., Angelopoulos, V., & Lu, Q. (2018). Intense cross-tail field-aligned currents in the plasma sheet at lunar distances. *Geophysical Research Letters*, *45*(10), 4610–4617. https://doi.org/10.1029/2018GL077902

Zaitsev, I., Cozzani, G., Alho, M., Horaites, K., Zhou, H., Kit, A., et al. (2025). Ion-mediated tearing and kink instabilities in the Earth's magnetosphere: Hybrid-Vlasov simulations. *Journal of Geophysical Research: Space Physics*, *130*(1), e2024JA032615. https://doi.org/10.1029/2024JA032615

Zelenyi, L. M., Artemyev, A. V., & Petrukovich, A. A. (2010). Earthward electric field in the magnetotail: Cluster observations and theoretical estimates. *Geophysical Research Letters*, *37*(6), 6105. https://doi.org/10.1029/2009GL042099

Zelenyi, L. M., Malova, H. V., Leonenko, M. V., Grigorenko, E. E., & Popov, V. Y. (2022). Equilibrium configurations of super-thin current sheets in space plasma: Characteristic scaling of multilayer structures. *Journal of Geophysical Research: Space Physics*, *127*(11), e2022JA030881. https://doi.org/10.1029/2022JA030881

Zhang, C., Rong, Z., Zhang, L., Gao, J., Shi, Z., Klinger, L., et al. (2023). Properties of flapping current sheet of the martian magnetotail. *Journal of Geophysical Research: Space Physics*, *128*(4), e2022JA031232. https://doi.org/10.1029/2022JA031232

Zharkova, V. V., Arzner, K., Benz, A. O., Browning, P., Dauphin, C., Emslie, A. G., et al. (2011). Recent advances in understanding particle acceleration processes in solar flares. *Space Science Reviews*, *159*(1–4), 357–420. https://doi.org/10.1007/s11214-011-9803-y